The Doppler Lidar Simulation Model (DLSM)

by

S. Wood, D. Emmitt, L. Wood and S. Greco

1.0 Overview

The Doppler Lidar Simulation Model (DLSM) is an evolution of existing Doppler lidar simulation models (Wood et al., 2014; Wood et al., 2000; Emmitt and Wood, 1996; Wood et al., 1995; Wood et al.,1993, Emmitt et al.,1990; Emmitt and Wood, 1988) that are currently used for spaced-based and airborne Doppler lidar wind simulations (Riishojgaard et al., 2012; Masutani et al, 2006; Lord et al, 2002; Emmitt and Wood, 2001; Wood et al., 2001; Greco et al., 2000; Wood et al., 1997; Atlas and Emmitt, 1995; Emmitt and Wood, 1995).The DLSM provides an interactive simulation that allows a user to address issues ranging from lidar system trade studies to global numerical model assimilation and impact studies with an emphasis on sampling in cloudy environments.

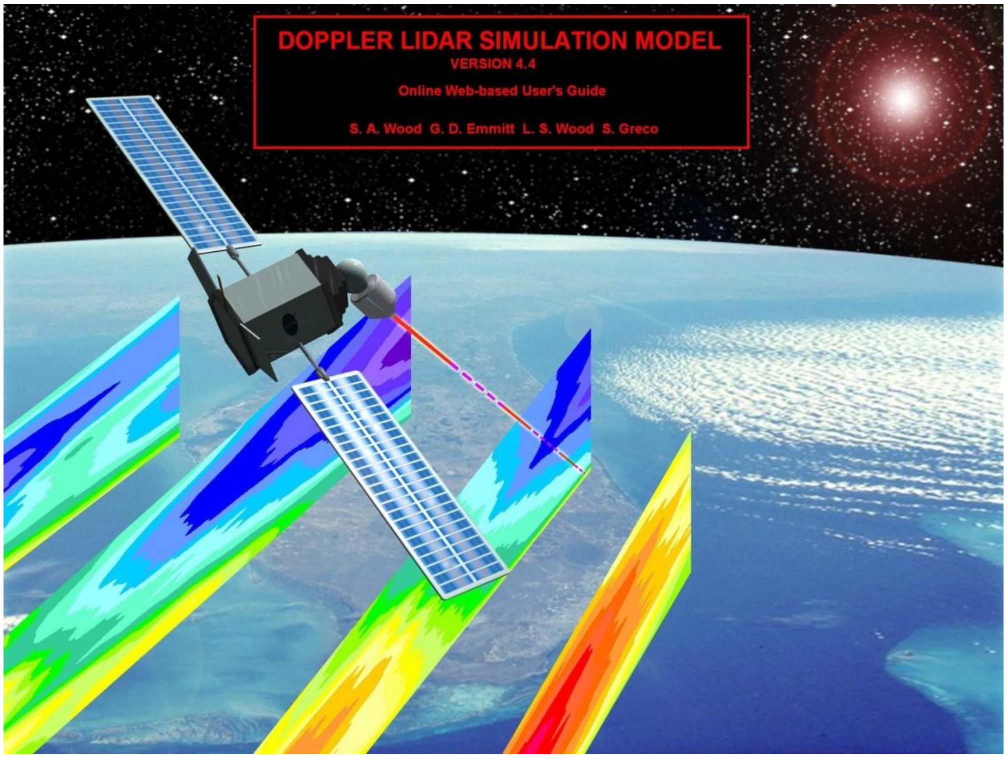

The DLSM version 4.4 recent upgrades include an Autocovariance Lidar sensor algorithm, support for ECMWF T511 and WRF nature run atmospheres, day/night effects, a slewing platform, redistribution of aerosols in the PBL via the PBL height, redistribution of aerosols in the stratosphere via tropopause height and platform/shot coverage from Satellite toolkit (Analytical Graphics, Inc).

SWA has created 120 days of Global Atmospheric Data Sets (GADS) based on the ECMWF T511 nature run and 10 days of Meso-scale Atmospheric Data Sets (MADS) based on the AOML WRF nature run via the Atmospheric Generator Model (AGM). The GADS and MADS are part of the DLSM's atmospheric library for simulations.

After internal discussions and review of several methods for incorporating multiple scattering effects, SWA decided that these effects would be very small for the FOVs contemplated for any future space based lidar. The expected information advantage did not merit the overhead to include multiple scattering effects (e.g. cloud ice particle habits).

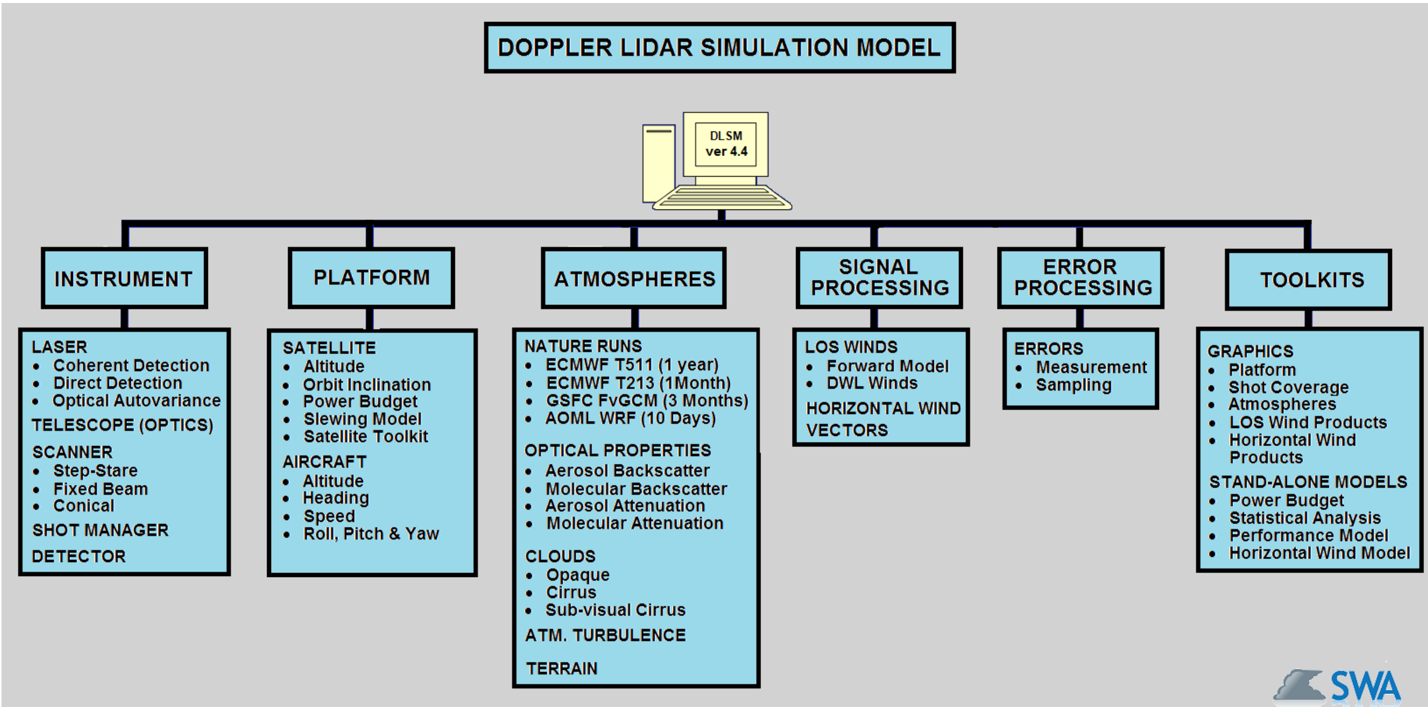

1.1 Computer System Description

1.1.1 HARDWARE/OPERATING SYSTEM

The DLSM was originally designed to run on a MS Windows 2000 terminal server via network or as a deliverable series of DVDs operating under the MS Windows 2000/XP operating system. In 2010, the model was ported to a Windows 7 operating system environment on a dual processor Dell PC.

1.1.2 DLSM SYSTEM ARCHITECTURE AND PROGRAMMING LANGUAGES

All DLSM inputs and graphic routines are coded in MS Visual Basic 6.0. The Lidar Simulation Model and Shot Coverage Model are coded in FORTRAN 90/95 using Compaq Visual Fortran professional edition 6.6. It is intended to upgrade the DLSM to run under Intel Fortran in 2014.

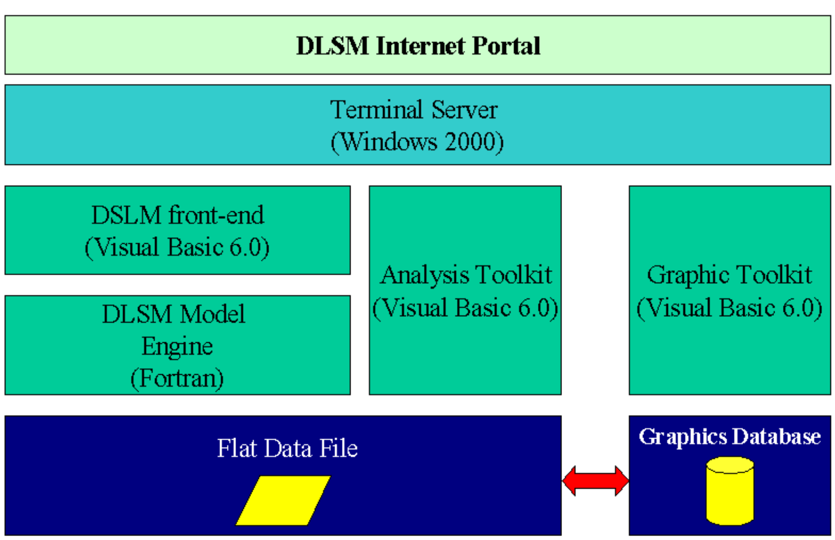

1.2 DLSM EXECUTION

Execution of the DLSM invokes the DLSM Main Screen: the model's control screen.

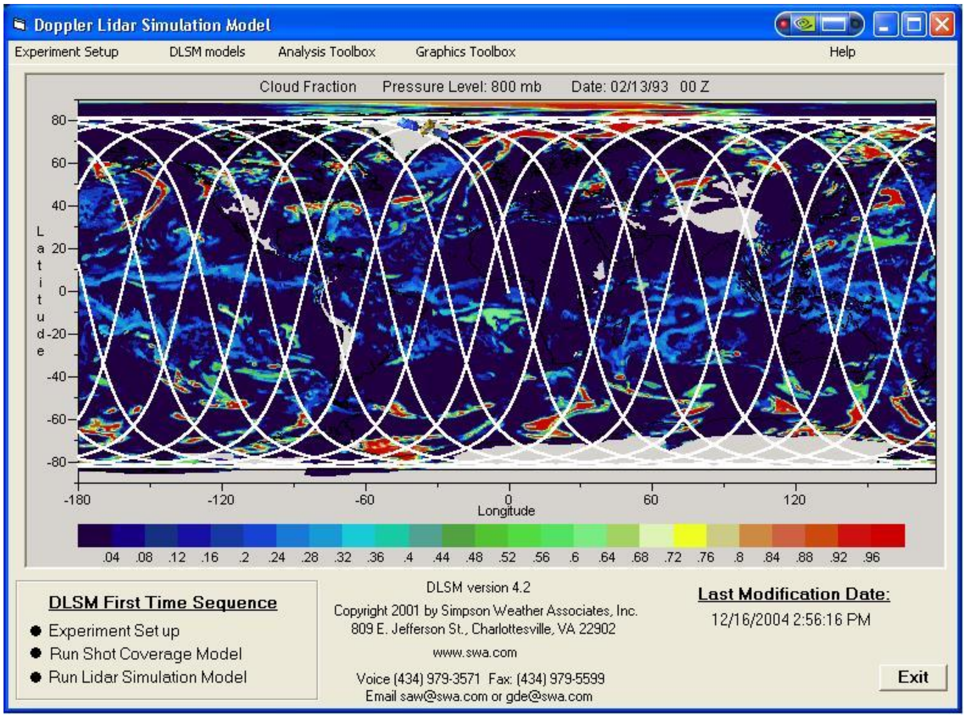

The DLSM Main Screen has five options: Experiment Manager, DLSM Models, Analysis Toolbox, Graphics Toolbox and Help.

For a first time user, the user should click on the Experiment Setup top menu option. This will invoke the Experiment Manager where the user customizes model inputs for a Mission Scenario. A Mission Scenario is defined as the platform/lidar inputs, atmospheric inputs, and simulation time block inputs. From the Experiment Manager, the user enters the necessary inputs to run the DLSM Fortran models, reviews inventory of past input files, loads existing files, and edits existing files. Once model inputs have been set up, the user should choose to run the Shot Coverage Model from the DLSM models menu which will create a global coverage data file of lidar shot information. Next, the user should choose to run the Lidar Simulation Model from the DLSM models menu which, in liaison with the shot coverage file and atmospheric inputs, will produce simulated lidar products. The DLSM models menu also allows the user to review the last processing message from the SCVM or LSM.

From the DLSM's Analysis Toolbox menu, the user can produce global statistics on the DWL line of sight wind results via the Performance Graphic Model. The Graphics Toolbox allows the user to graph platform coverage, lidar shot coverage, three dimensional atmospheric variables, simulated lidar products and corresponding errors.

2.0 LIDAR SIMULATION MODEL TECHNICAL

The Lidar Simulation Model (LSM) (Emmitt and Wood, 1996; Wood et al., 1995) is an evolution of existing Doppler lidar simulation models (Wood et al., 1993; Emmitt et al., 1990) that are currently used for spaced-based Doppler lidar wind simulations (Lord et al, 2002; Wood et al., 2001; Baker et al., 1995) and airborne Doppler lidar wind simulations (Wood et. al., 1997). The LSM is a fully integrated Doppler lidar simulation model that produces simulated lidar winds and corresponding errors using either global or mesoscale atmospheric model wind fields. The LSM can address various types of questions on the feasibility and optimal functionality of a space-based or airborne Doppler lidar system. The LSM is also designed to address engineering trades, measurement accuracies (line of sight and horizontal wind vector), measurement representativeness, resolution and areal coverage.

2.1 SATELLITE AND DWL SHOT COVERAGE

2.1.1DWL SHOT COVERAGE MODEL

The Shot Coverage Model (SCVM) is a stand-alone FORTRAN 90 model that allows the user to simulate satellite and aircraft missions with a variety of laser scanner patterns. The SCVM provides ASCII records of platform track and laser shot coverage (spatial and temporal) for the LSM.

2.1.1.1 SATELLITE MODEL

The satellite model provides the satellite latitude and longitude and the inclination angle of the orbit as a function of orbital time. The satellite model solves an oblique spherical triangle algorithm (Kells, et al, 1940) to compute the satellite location. The model assumes a spherical earth. Currently the SCVM forces the starting latitude to be at the equator while the user may choose any longitude.

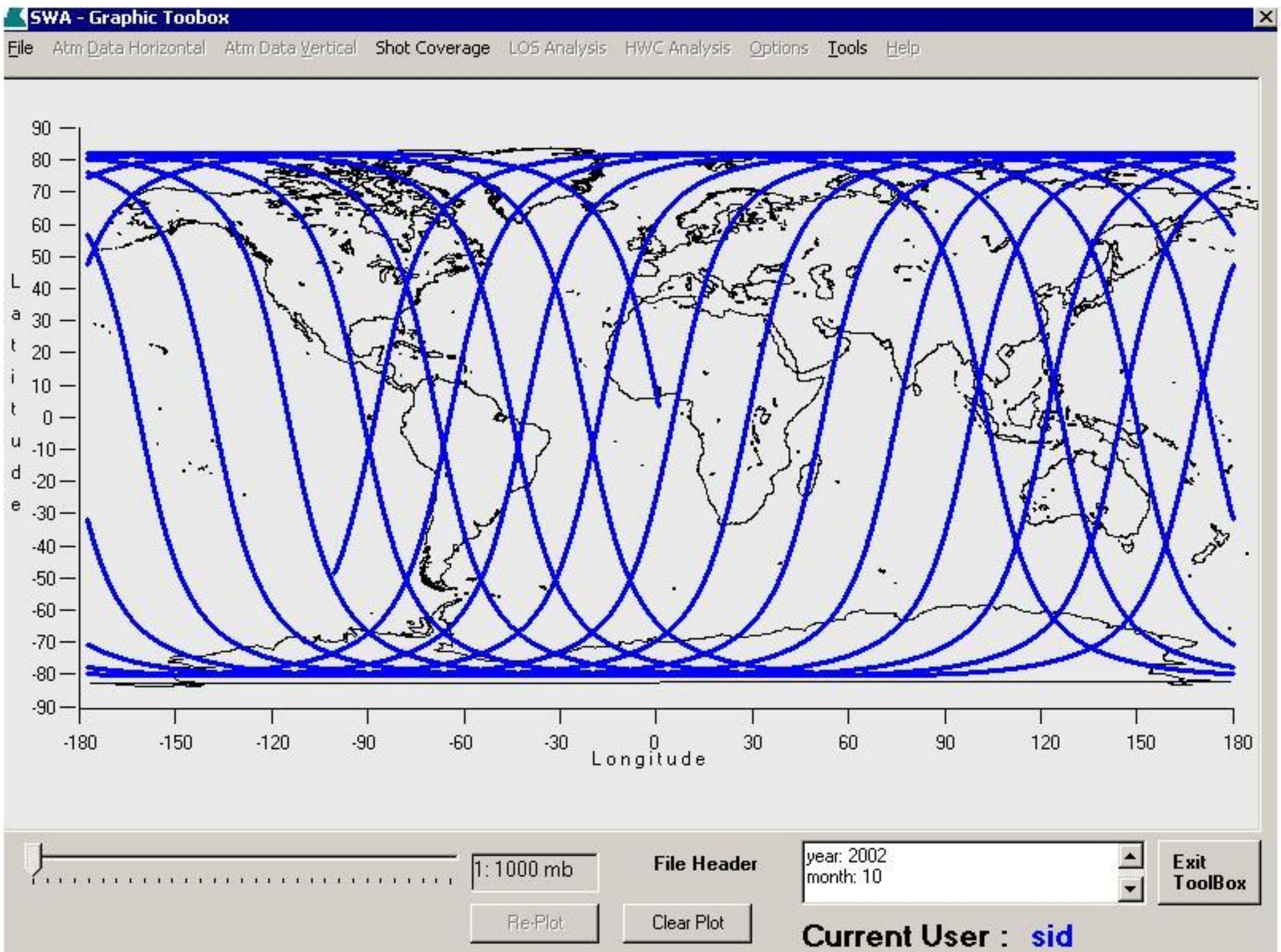

The speed of the satellite is computed as

$$V_{sat} = ((Gearth/(R_e + Z_s))^{1/2})$$

where

variable	units	definition	pre-set value
V_{sat}	(km/s)	satellite velocity	----
Gearth		constant	39.9251e4
Z_s	(km)	satellite altitude	----
R_e	(km)	equatorial radius of earth	6371.22

2.1.1.2 AIRCRAFT MODEL

The aircraft model reads in an existing aircraft data file containing aircraft altitude, location, heading, and attitude information as a function of time along a flight path. The aircraft data files can be real missions or simulated ones. There are 23 aircraft data files in the SCVM inventory, 21 real and two simulated. The SCVM allows the user to adjust the flight track, vertically and horizontally, on the globe.

2.1.1.3 SCANNER MODEL

The scanner model uses the platform latitude and longitude to compute the latitude and longitude of each lidar shot as a function of the laser pulse (range), nadir scan angle and azimuth scan angle. The model uses an oblique spherical triangle algorithm (Kells, et. al, 1940) that solves for a spherical triangle defined by the north pole, the position of the satellite and the position of the shot. The Shot Coverage Model (SCVM) supports conical, fixed and step-stare scanners.

2.1.1.3.1 Scanner System Geometry

The scan geometry angles and swath width are computed as shown below

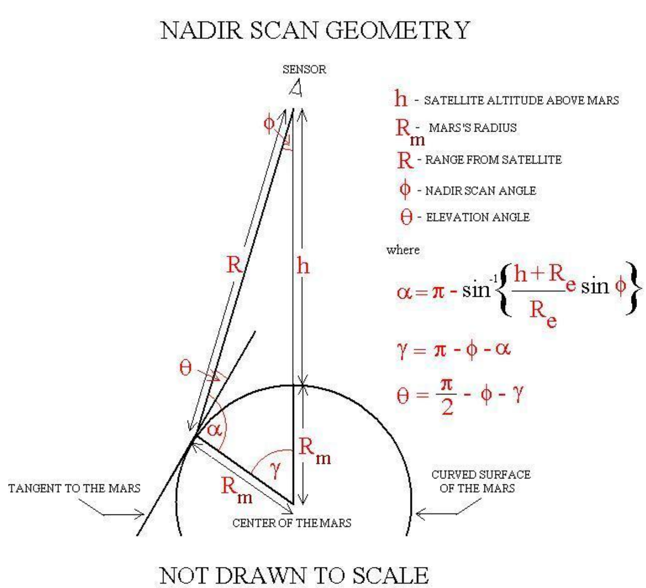

$$SW = 2 \cdot \gamma/360 \cdot 2 \cdot \pi \cdot R_e$$

where

variable	units	definition	pre-set value
α	rad	satellite to shot to center of the planet angle	----
π	rad	the constant, PI	3.14159
Z_s	km	satellite altitude	----
R_m	km	equatorial radius of Earth	6371.22
ϕ	rad	nadir scan angle	----
γ	rad	satellite to planet's center to shot angle	----
Θ	rad	slant path elevation angle	----
SW	km	swath width distance	----

2.1.1.3.2 CONICAL SCANNER

The conical scanner gives the latitude and longitude of the lidar shot and the azimuth scan angle for a counter-clockwise scanning lidar.

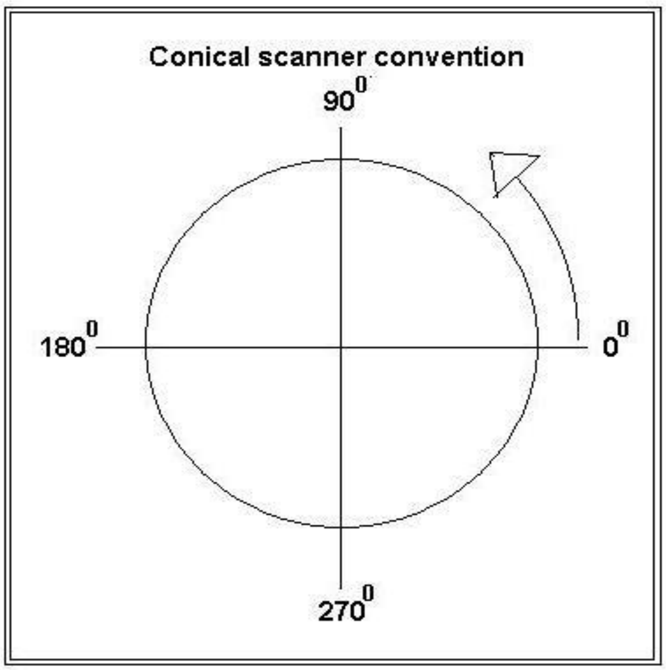

The user can apply a cosine modification to the conical scan.

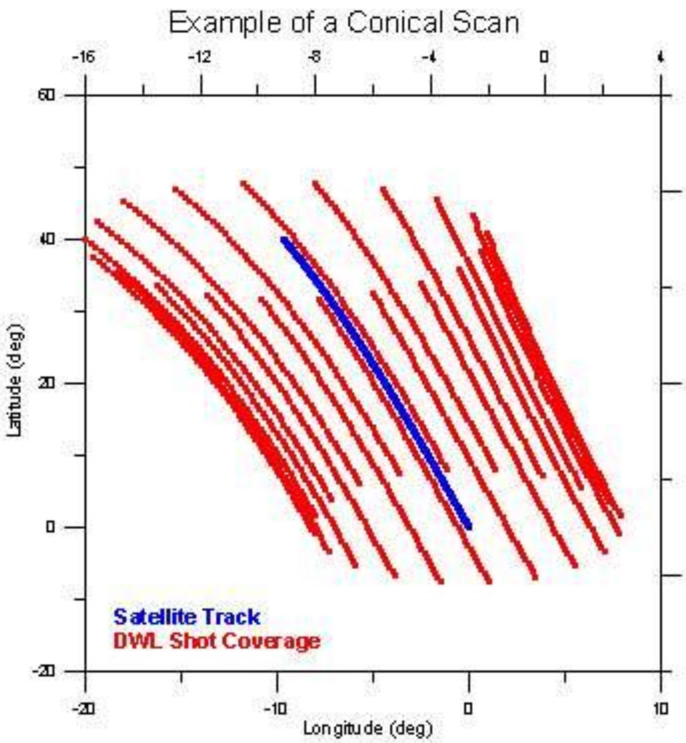

Starting altitude of the satellite (km): 833.00
Starting orbit inclination angle (deg): 98.00'
Peak prf of the scanner (hz): 12.00
Nominal prf of system (hz): 12.00
Starting orbit inclination angle (deg): 98.00
Peak prf of the scanner (hz): 2.00
Nominal prf of system (hz): 2.00
Scanner shot manager type: Conical
Diameter of the primary telescope mirror (m): 0.75
Nadir scan angle (deg): 45.00
Scanner rate (rpm): 6.00
Pointing jitter (uRad): 0.00
PRF option: use nominal prf
Cosine modulation option: no modulation

2.1.1.3.3 *STEP-STARE*

The Step-Stare scanner gives the latitude and longitude of the lidar shot for up to twenty telescope azimuth dwell angles. Each telescope is configured with a laser firing dwell time and a prf associated at a fixed azimuth. Also included is a laser firing in-between the fixed beam dwells parameterized by a gap time and prf associated with a clockwise or a counter-clockwise conical scan. A complete scan pattern is defined as the scan patterns for all the user's telescope azimuths plus the in-between gaps. A duty cycle is used to define a wait time before the complete scan pattern is repeated as calculated below.

$$\text{cycle wait time} = \text{complete scan pattern} - \text{complete scan pattern} \times \text{duty cycle} / 100.0$$

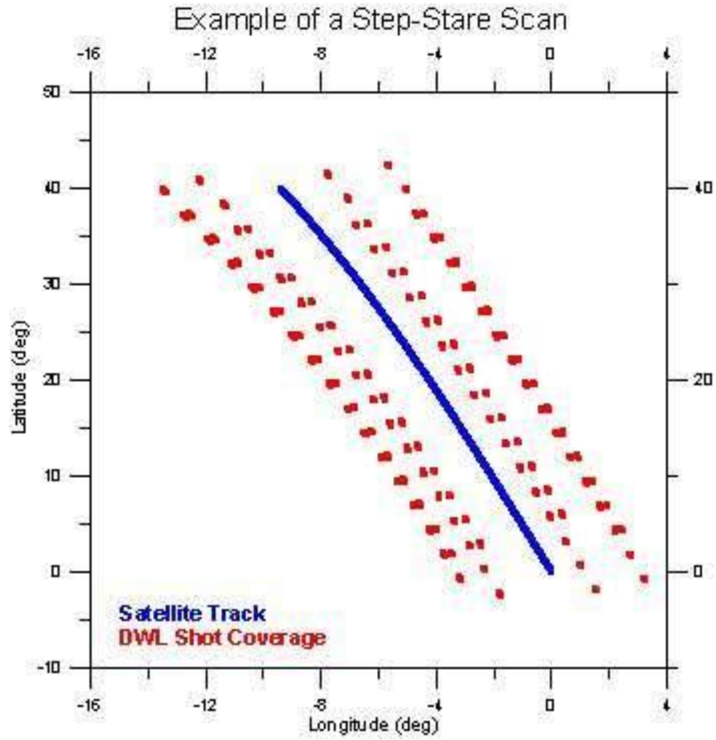

Starting altitude of the satellite (km): 400.00
Starting orbit inclination angle (deg): 98.00'
Peak prf of the scanner (hz): 12.00
Nominal prf of system (hz): 12.00
Starting orbit inclination angle (deg): 98.00
Peak prf of the scanner (hz): 12.00
Nominal prf of system (hz): 12.00

Number of discrete azimuths: 08

Sequence of discrete azimuths		1	2	3	4	5	6	7	8
Fixed/step-stare discrete azimuth angle	deg	123	147.8	327.80	237.	291.30	212.20	32.20	68.70
Nadir scan angle for each azimuth angle	deg	45	45	45	45	45	45	45	45
Time for a fix/s beam to fire shots	s	5	5	5	5	5	5	5	5
Time between fix/ss beam shot patterns	s	0	0	0	0	0	0	0	0
Discrete azimuth dwell PRF option flag		peak prf	peak prf	peak prf	peak prf	peak prf	peak prf	peak prf	peak prf
Discrete azimuth gap PRF option flag		peak prf	peak prf	peak prf	peak prf	peak prf	peak prf	peak prf	peak prf
Direction scan to next fix/ss beam azimuth		CW	CW	CW	CW	CW	CW	CW	CW

Duty cycle of the scan pattern (%): 100.00

2.1.2 SATELLITE TOOLKIT

In 2012, an option was added to the DLSM to support coverage input files from Satellite Toolkit (Analytical Graphics, Inc). STK was used to generated equatorial space station and DWL shot location records for four month period (July-Oct 2005). The data sets had additional satellite slewing information for adaptive targeting simulations where the satellite can rotate allowing DWL line of sight to reach areas of high interest. Also included is a day/night flag for the OAWL and direct detection systems.

Shot Coverage Model Output records

Variable Record	units
Satellite latitude	(deg)
Satellite longitude	(deg)
Time laser shot was taken	(s)
Azimuth scan angle	(deg)
Sequence number of azimuth angle	#
Satellite heading	(deg)
Platform Altitude	(km)
Number of altitude levels (0 for satellite)	#
Nadir scan angle	(deg)
Scan pattern indicator 0-conical 1-stare 2-gap	
Satellite Roll (STK only)	(deg)
Laser shot latitude f(z)	(deg)
Laser shot longitude f(z)	(deg)
Laser shot altitude f(z)	(deg)
Orbit quadrant indicator f(z)	
Day/Night Flag (STK only) 0 - night 1 - day	

2.2 ATMOSPHERIC LIBRARY

The LSM's atmospheric library is made up of an extensive set of integrated atmospheric data bases created by the Atmospheric Generator Model (AGM). The library can provide meteorological inputs from control fields, generated fields, mesoscale fields to global meteorological fields. The library includes opaque clouds, cirrus clouds, aerosol backscatter, molecular and aerosol attenuation, atmospheric turbulence and terrain. The AGM can create two types of atmospheric files: Global Atmospheric Data Set (GADS) and Mesoscale Atmospheric Data Set (MADS).

2.2.1 GLOBAL ATMOSPHERIC DATA SETS AND MESOSCALE ATMOSPHERIC DATA SETS

The Atmosphere Generator Model (AGM) creates Global Atmospheric Data Sets (GADS) that the LSM uses for global type simulations and Mesoscale Atmospheric Data Sets (MADS) for regional type simulations. The LSM retrieves atmospheric profiles as a function of latitude and longitude for each laser shot. Each profile contains a Nature Run atmospheric inputs, aerosol and molecular optical properties, sub-grid scale turbulence, cloud information and terrain. The LSM linearly interpolates in time and space to estimate the atmospheric variables for each DWL measurement. GADS and MADS are a FORTRAN 90/95 direct access files created by using the Nature Run data in liaison with the AGM optical property models, cloud models, and terrain data set. 2013 Inventory of the atmospheric library consists of GADS based on T511 ECMWF Nature Run for 7/1/2005 - 10/31/2005 and MADS based on AOML WRF 8/1/2005 - 8/10/2005 at the grid resolutions of 27, 9, 3 and 1 km.. A new ECMWF Nature Run, T1148, is being consider for future OSSE. Past GADS for NASA/GSFC's FvGCM, ECMWF's T213 and T106 and past MADS for RAMS Nature Run for 2/11/93 - 1/21/93 and eta 6/4/95 have been retired.

Atmospheric Data Base Records

GADS VARIABLES	MADS VARIABLES
Latitude (deg)	Latitude (deg)
Longitude (deg)	Longitude (deg)
Total Cloud Amount (%)	Surface Pressure (mb)
High Cloud Amount (%)	Terrain Height (M)
Medium Cloud Amount (%)	Surface Type flag (0-water, 1-land)
Low Cloud Amount (%)	Planetary Boundary Layer (M)
Surface pressure (mb)	Horizontal Wind Component U Ten Meter (M/S)
Mean Sea Level Pressure (mb)	Horizontal Wind Component V Ten Meter (M/S)
Geopotential Height at SFC (m)	Time Step Cumulus Precip.
Surface Type flag (0-water, 1-land)	Time Step Non-Convective Precip.
Planetary Boundary Layer (M)	Accumulated Total Cumulus Precip.
Horizontal Wind Component U Ten Meter (M/S)	Accumulated Total Grid Precip.
Horizontal Wind Component V Ten Meter (M/S)	Albedo (0-1)
Large Scale Perecip. Rate (m)	Air Temperature profile (k)
Convective Precip. Rate (m/3 hr)	Horizontal Wind Component U profile (M/S)
Stratiform Precip. Rate (m/3 hr)	Horizontal Wind Component V profile (M/S)
Sea Surface Temperature (K)	Vertical Velocity profile (Pa/S)
Albedo (0-1)	Cloud Fraction profile (%)
Surface Roughness (m)	Atm. Pressure (mb)
Air Temperature profile (k)	Geopotential Height profile (m)
Horizontal Wind Component U profile (M/S)	Vapor Mixing Ratio profile (KG/KG)
Horizontal Wind Component V profile (M/S)	Cloud Mixing Ratio profile (KG/KG)
Specific Humidity profile (%)	Ice Mixing Ratio profile (KG/KG)
Vertical Velocity profile (Pa/S)	Snow Mixing Ratio profile (KG/KG)
Cloud Liquid Water Content profile (KG/KG)	Graple Mixing Ratio profile (KG/KG)
Cloud Ice Water Content profile (KG/KG)	
Cloud Fraction profile (%)	
Geopotential Height profile (m)	
Divergence profile (s-1)	
Vorticity profile (s-1)	
Ozone Mass Mixing Ratio profile (KG/KG)	
Atm. Pressure profile (mb)	
Relative Humidity profile (%)	Relative Humidity profile (%)
Space View Of Cloud Fraction profile (%)	Space View Of Cloud Fraction profile (%)
Cloud Type profile	Cloud Type profile
Sub-grid Scale Turbulence in U profile (M/S)	Sub-grid Scale Turbulence in U profile (M/S)
Sub-grid Scale Turbulence in V profile (M/S)	Sub-grid Scale Turbulence in V profile (M/S)
Sub-grid Scale Turbulence in W profile (M/S)	Sub-grid Scale Turbulence in W profile (M/S)
Aerosol Backscatter profile varying around Background Median log(m-1 sr-1)	Aerosol Backscatter profile varying around Background Median log(m-1 sr-1)
Aerosol Backscatter profile varying around Enhanced Median log(m-1 sr-1)	Aerosol Backscatter profile varying around Enhanced Median log(m-1 sr-1)
Aerosol Scattering profile varying around Background Median log(m-1 sr-1)	Aerosol Scattering profile varying around Background Median log(m-1 sr-1)
Aerosol Scattering profile varying around Enhanced Median log(m-1 sr-1)	Aerosol Scattering profile varying around Enhanced Median log(m-1 sr-1)

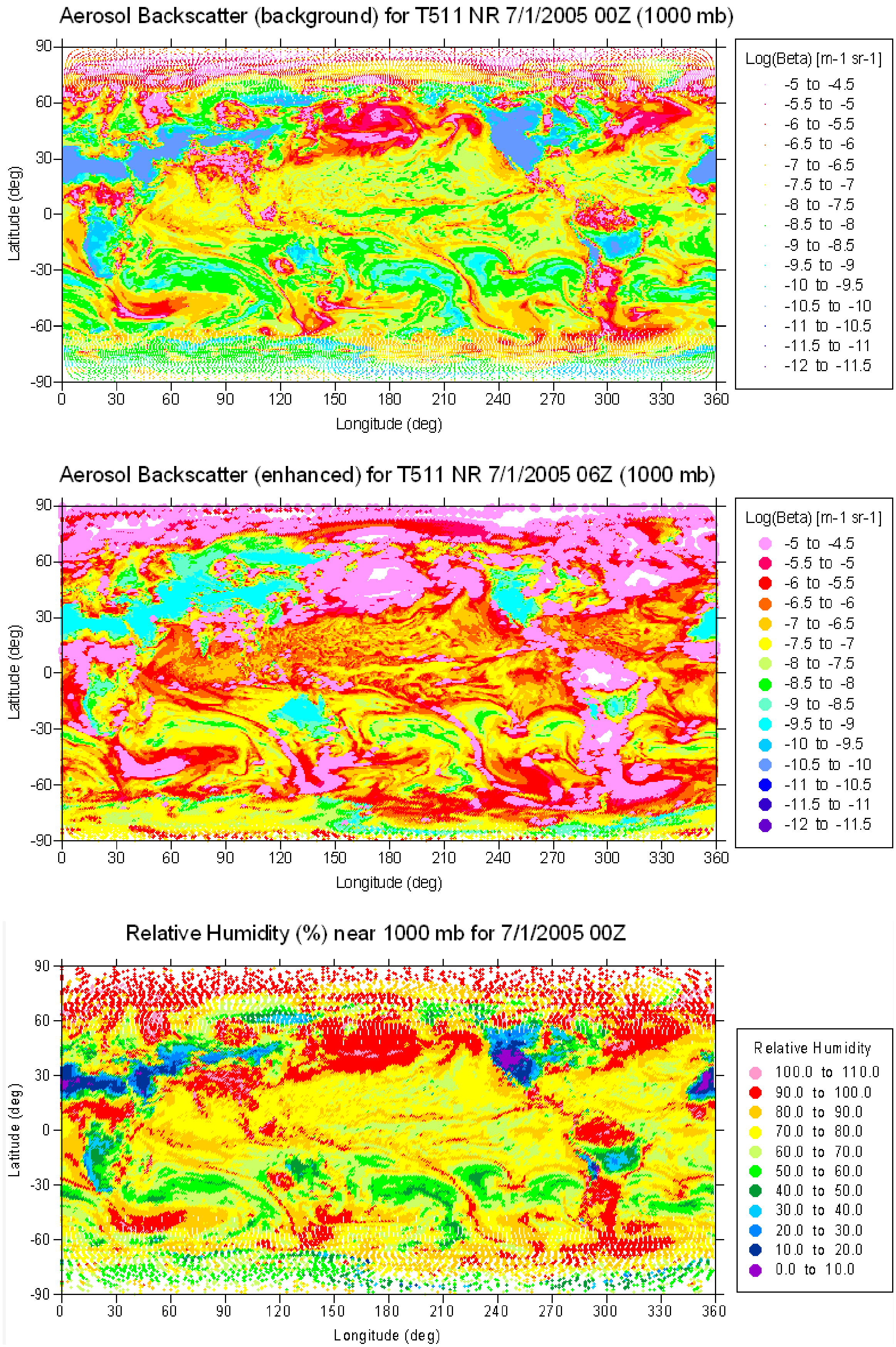

Figure 1. Enhanced and background ECMWF dependent aerosol backscatter fields for 1000 mb. The backscatter was organized by relative humidity.

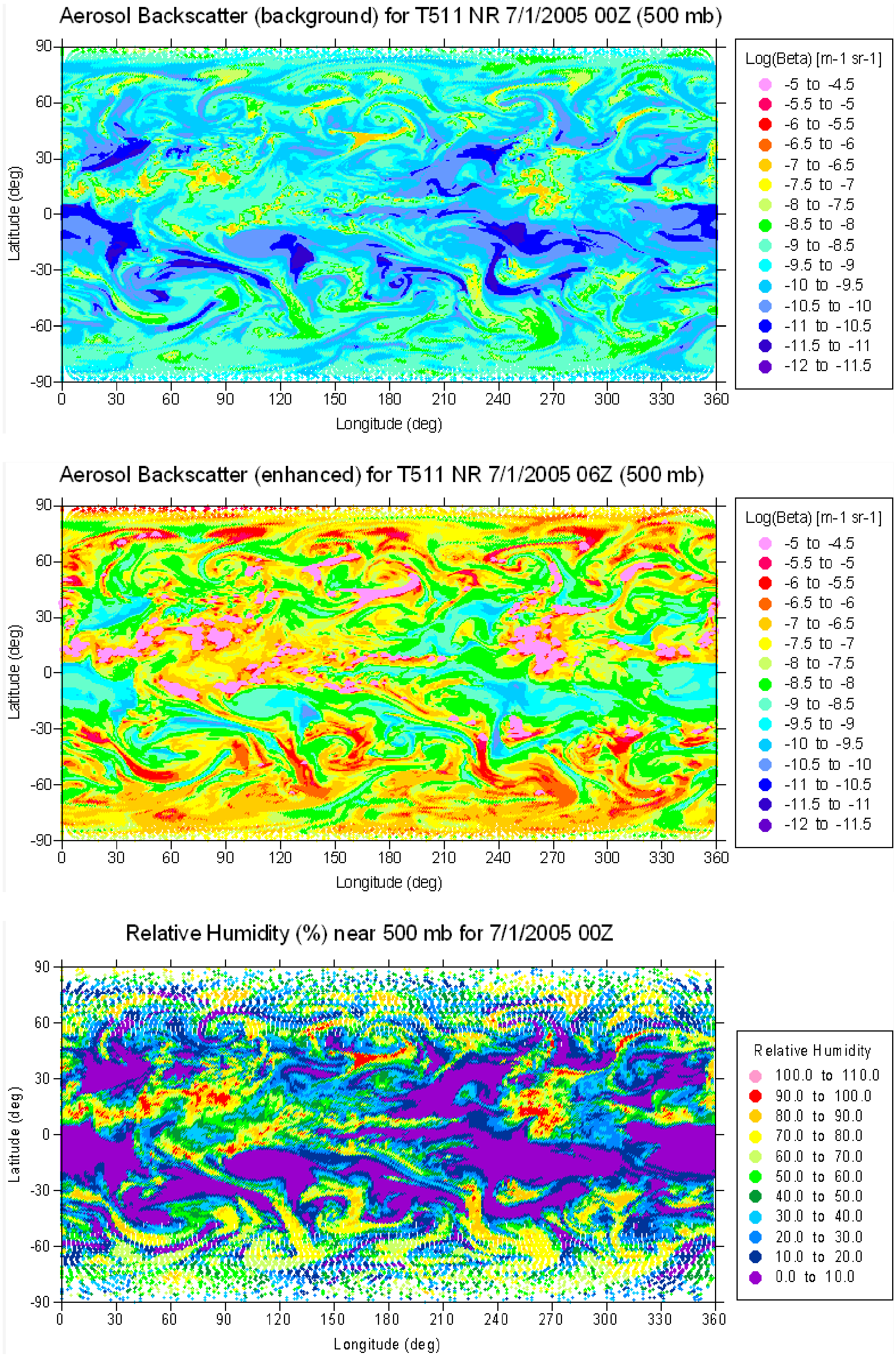

Figure 2. Enhanced and background ECMWF dependent aerosol backscatter fields for 500 mb. The backscatter was organized by relative humidity

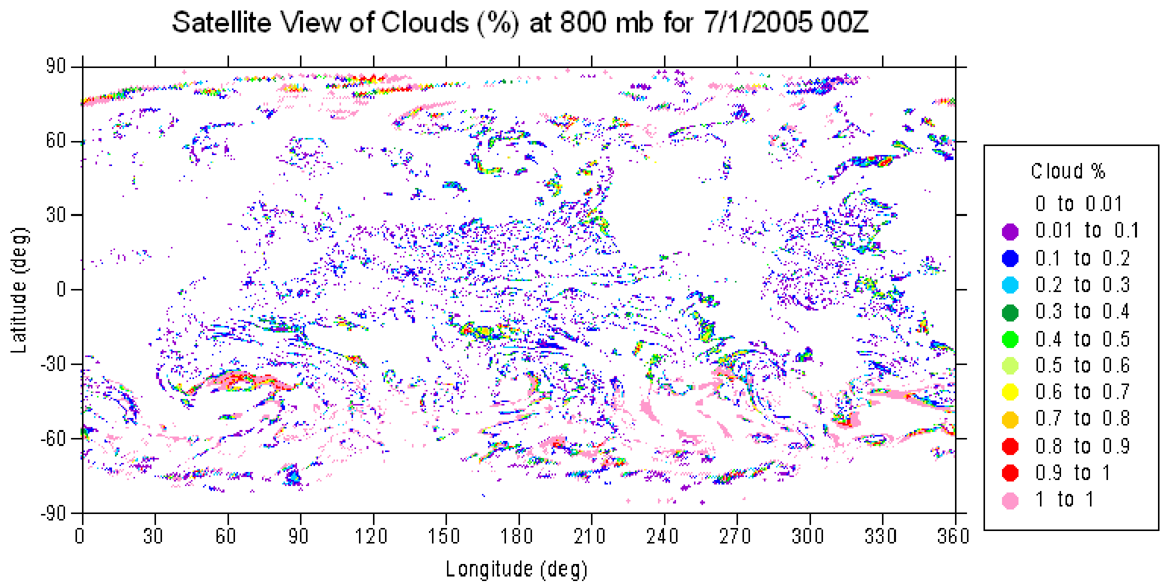

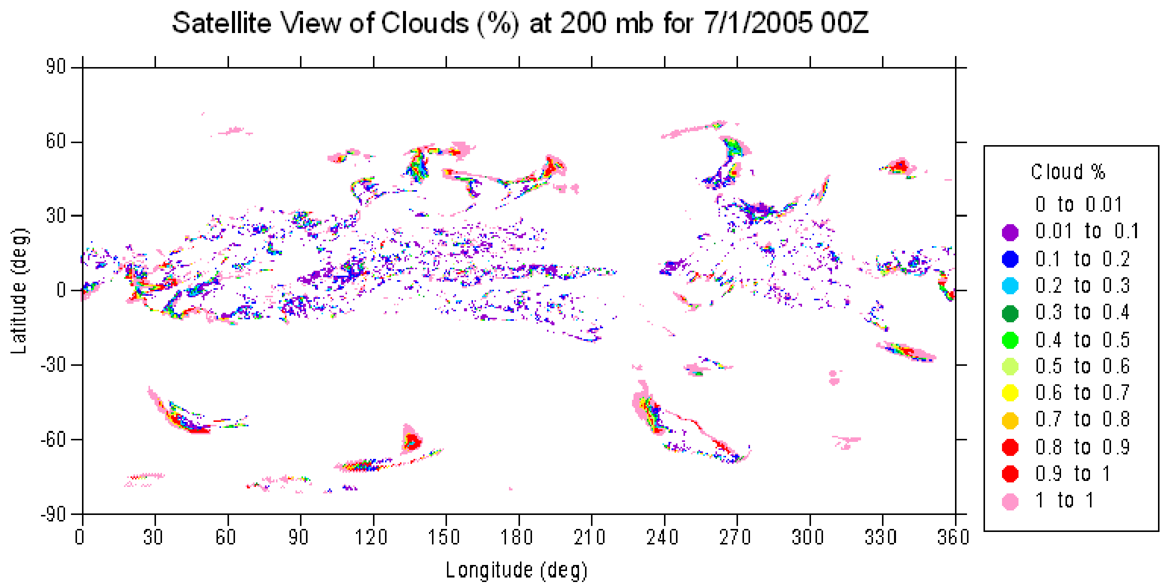

Figure 3. Satellite view of clouds at 800 and 200 mb for ECMWF T511 nature run 07/01/2005 00Z.

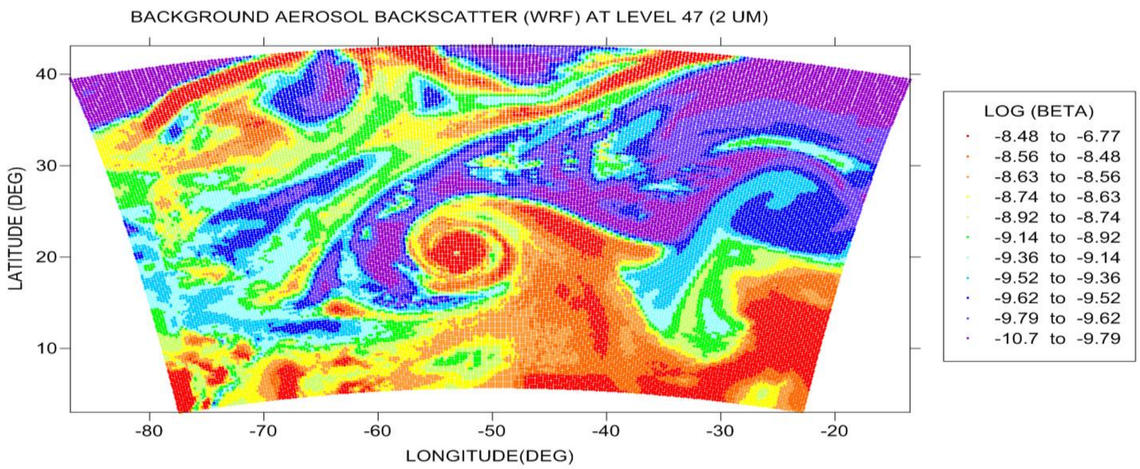

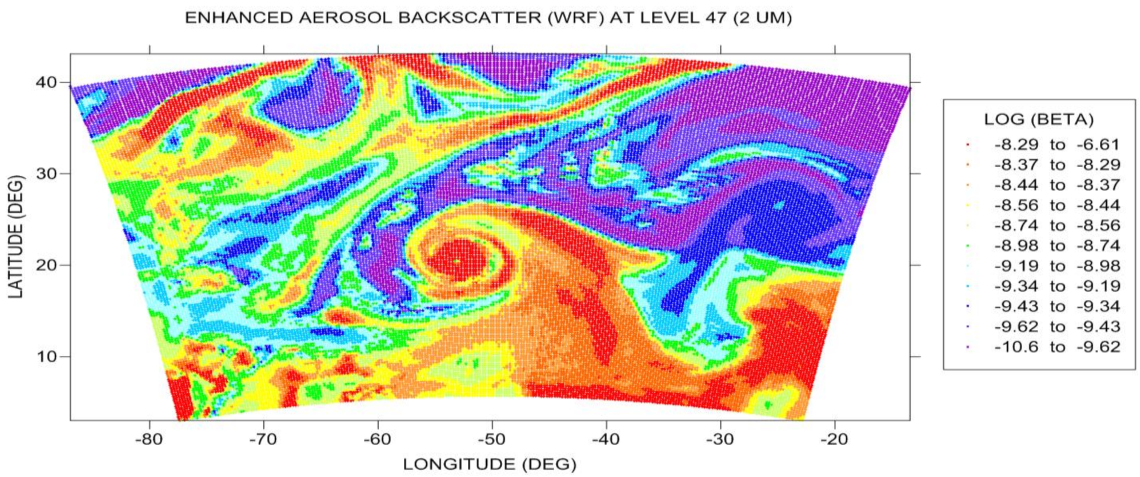

Figure 4. Enhanced and background WRF dependent aerosol backscatter fields for level 47. The backscatter was organized by relative humidity.

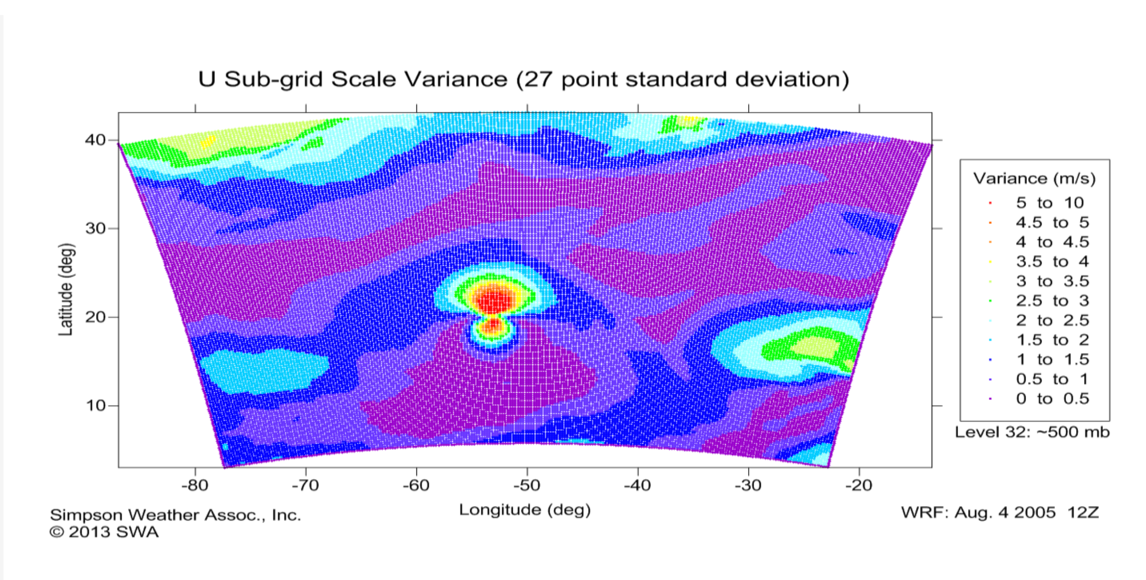

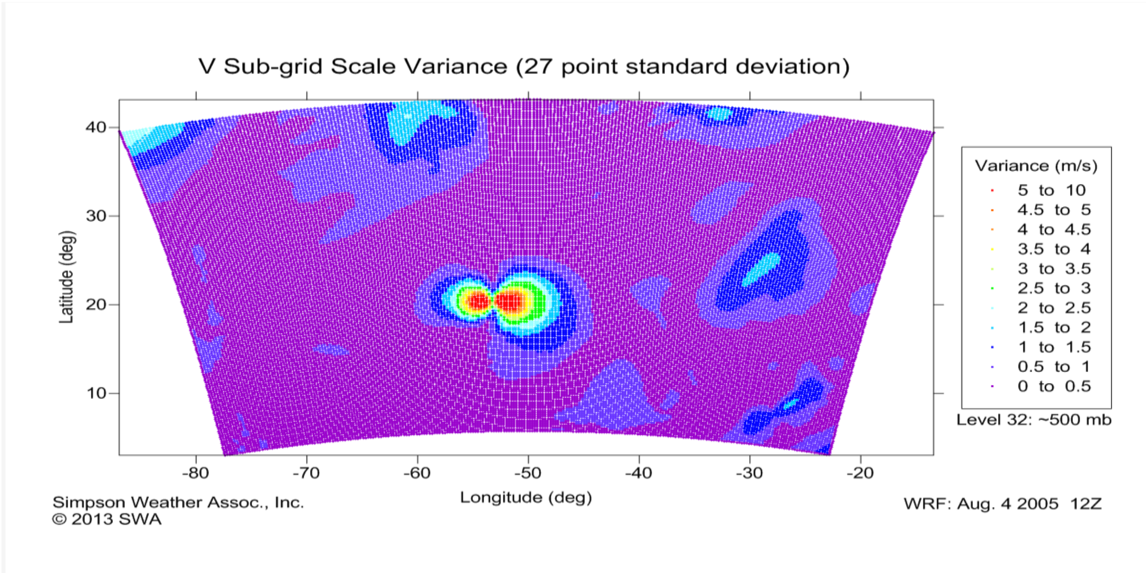

Figure 5. WRF Sub-grid scale turbulence for the U and the V wind components for 08/04/2005 12Z.

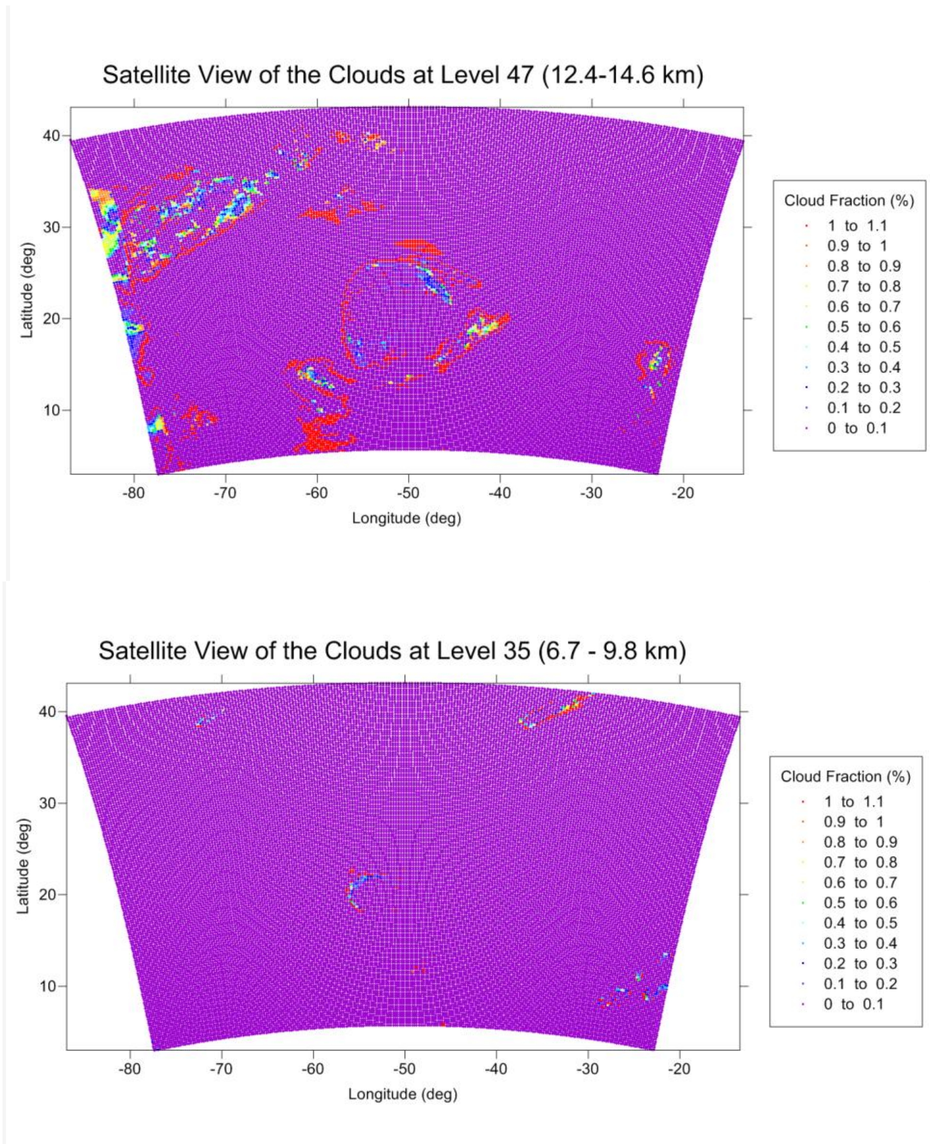

Figure 6. WRF Satellite view of cloud for levels 35 and 47 for 08/04/2005 12Z.

2.2.2 OPTICAL PROPERTY MODELS

The DLSM version 4.4 optical property models are currently based upon the Design Atmospheres for use in GTWS Concept Studies provided by the Science Definition Team for the NASA/NOAA Global Tropospheric Wind Sounder.

Having a common scattering target with internally consistent backscatter wavelength dependence enables meaningful "equal resource/equal target" comparisons of GTWS concepts that employ Doppler lidars. While the Science Definition Team (SDT) realizes that aerosol backscatter from the atmosphere will vary over several orders of magnitude, will vary over altitude, latitude and season and will also vary over space/time scales that are not readily modeled, the GLOBE, SABLE/GABLE backscatter surveys, and the AFGL FASCODE aerosol data bases provide a nearly consistent picture of backscatter climatology.

To establish a set of bounding profiles, the SDT has chosen (1) the "background" distribution of backscatter that appears in most stacked histograms of the GLOBE/SABLE/GABLE data sets and (2) the distribution of "enhanced" backscatter opportunities that are most apparent during the summer seasons and more common in the northern hemisphere (Srivastava, et al, 2001). The background mode value should not be interpreted as representing the minimum value of the aerosol cross section to be found. Rather, it represents a low cross section modal peak for aerosols in tropospheric air that does not have loading enhancement due to identifiable aerosol transport. There is a distribution of values and measurements indicating that the lowest aerosol cross sections can be an order of magnitude lower than the mode in some cases. The actual distribution of cross sections in the background mode are not well known. Measurements indicate that the background aerosol mode is present in large regions of the globe, mostly in the upper troposphere but can also be found in the boundary layer. The global distribution of these modes is not known, nor is the correlation of these modes with regions of ageostrophy.

The AGM provides background, enhanced and FASCODE optical property data bases for 0.355 µm, 0.532 µm, 1.06 µm and 2.0518 µm DWL wavelengths. The DLSM can choose the median profiles or to use the median profiles with aerosol backscatter randomly distributed with log normal variability as shown in the figure below. The DLSM uses the same random data seed for an entire DWL "shot's " line of sight path.

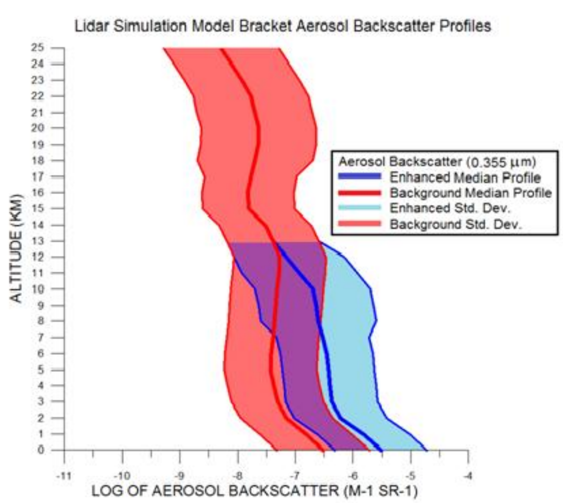

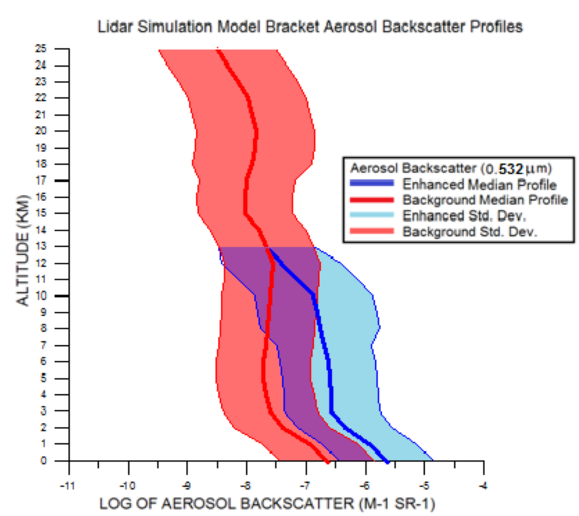

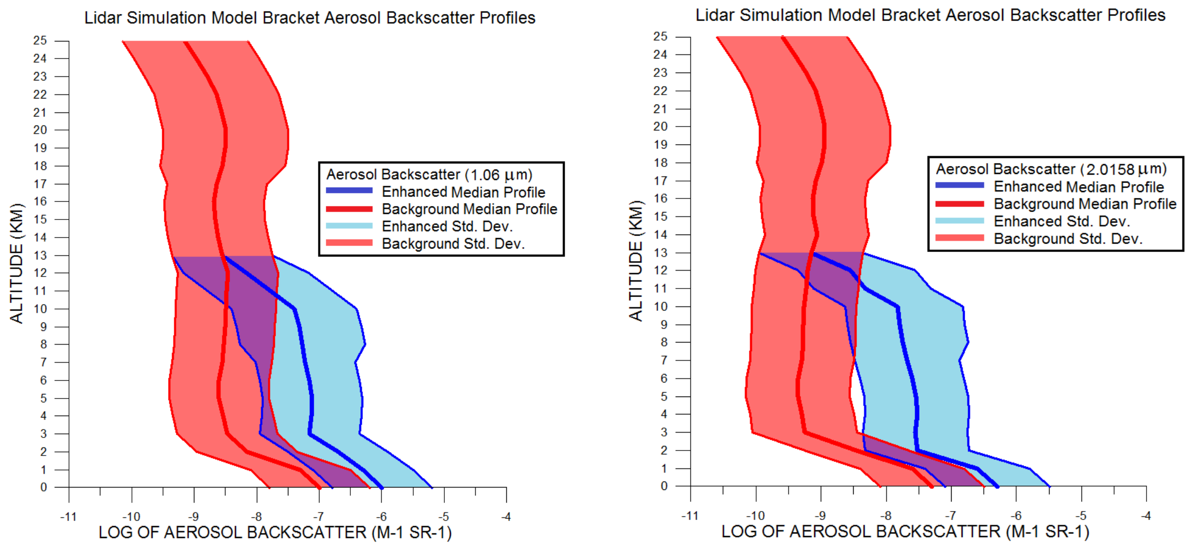

Figure 7 a, b, c, d. DLSM Probabilistic Aerosol Backscatter for 0.355, 0.532, 1.06 and 2.0159µm. Background and Enhanced modes based upon the GTWS Concept Studies Design Atmospheres.

The AGM uses nature run humidity fields to organize in 3-D the aerosol scatter and backscatter optical properties.

In past OSSE simulations of DWL observations, aerosol backscatter was taken from the PDF defined in the GTWS design reference atmospheres and assign to a given level in the atmosphere. Since those backscatter profiles are composites constructed from sets of airborne backscatter observations and represent PDFs for different layers in the atmosphere they make no assumption regarding temporal or spatial correlation. In 2013 SWA redistributed the PBL driven aerosols in a more physically realistic vertical representation. Since the PBL is a 1st order concentrator of aerosols generated at the earth's surface and the new Nature Runs output a PBL depth, the distribution of aerosols is described by a well mixed layer of constant backscatter defined by the model's PBL with a rapid vertical transition to the background (or enhanced) backscatter values. In the figure below, the vertical backscatter distribution around the median for a 24 hour OAWL (0.355 µm) simulation using the T511 nature run is shown for the background an enhanced aerosol modes.

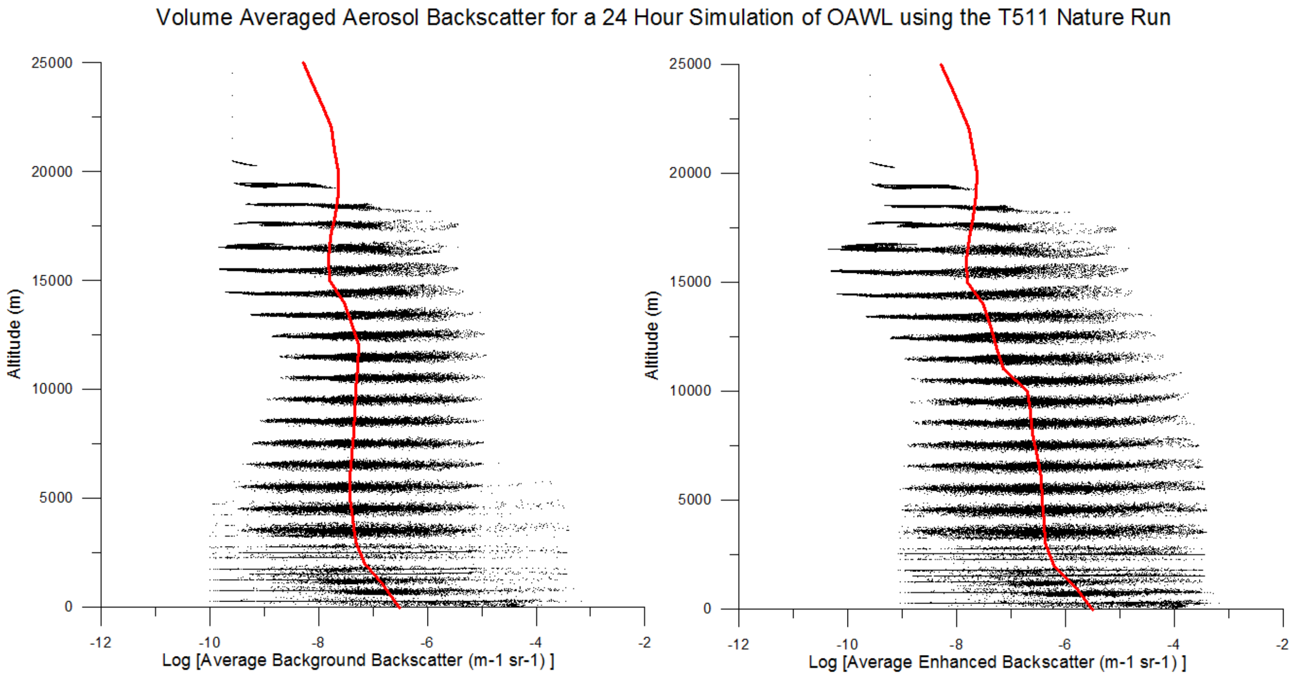

Figure 8. 24 hour Background and Enhanced Aerosol Backscatter distributions for the ECMWF T511 nature run.

2.2.3 CLOUD MODELS

Perhaps the most critical aspect of the DLSM is the representation of clouds along the line of sight of each DWL "shot". For any given detection sensitivity of the DWL, clouds will determine how often observations are made throughout the troposphere. The challenge is to accomplish reasonable cloud representation of backscatter, attenuation, porosity, multi-layering and multiple-scattering effects using the grid-point values of idealized 3-D numerical models.

2.2.3.1 NATURE RUN CLOUD FIELDS

The DLSM relies upon the cloud algorithms incorporated into the 3-D models. The cloud information (percentage, liquid water content, ice water content, horizontal location and vertical location) for T511 GADS and WRF MADS are obtained directly from the nature runs.

The DLSM does not claim to be valid on a shot to shot simulated performance. However, the model is designed to minimize the number of fixed cloud properties and to allow the user to vary the cloud properties in a way to test model's sensitivity to the line of sight perspective.

2.2.3.2 GLOBAL STATISTICS

We expect that clouds (including subvisual cirrus) will be in the field-of-view (FOV) of a space-based lidar 70-80% of the time. This estimate is based upon the recently reported analysis of two years of HIRS data (Menzel et al., 1992), the cirrus climatology derived from SAGE data by Woodbury and McCormick (1986) and the Nimbus-7 global cloud climatology (Stowe et al., 1989). Much of this cloud coverage is high cloud (above 400-500 mb) and is semi-transparent (~ 30-40%). Very thin or subvisual cirrus (ç <.07) is probably not detected by HIRS or Nimbus-7 but may be occasionally represented in the SAGE observations. Thus, we conclude that the occurrence of very thin cirrus is clearly underestimated in current climatologies.

Of particular interest to a space-based lidar program are the semi-transparent and optically thin clouds since they provide strong returns without full extinction (Emmitt and Wood, 1988). When one considers that the statistics given above are, in most cases, exclusive - i.e., they do not provide a good representation of coincident clouds at different altitudes, it is very likely that there are many occasions when there are multi-layers of thin clouds underlaid by opaque clouds.

SWA examines the distribution of total cloud coverage as a function of latitude for each nature run. While the total global coverage is reasonable when compared to Nimbus-7 statistics, we find that each model atmosphere tends to underestimates cloud cover.

2.2.3.3 CLOUD VERTICAL STRUCTURE MODEL

The LSM cloud vertical structure model constructs a vertical profile of cloud information from the platform's viewpoint given a vertical profile of a DWL " shot" locations along the slant path range (i.e. pulse length) and the 4-D interpolated GADS variables at the DWL " shot" locations.

As the model's loops from the top of the atmosphere to the surface of the earth, the following logic is used.

First, there has to be at least a 5 % cloud fraction for a cloud to be present at a level. Second, if there is a cloud present, the cloud is considered opaque unless the liquid water content is less than an LSM pre-set liquid water content threshold (currently set as 0.05 g/Kg) and the air temperature is less than an LSM pre-set air temperature threshold (currently set as 273K) , then the cloud is considered to be a cirrus cloud. If there is ice water content present, the cloud is considered to be cirrus.

If the cloud is cirrus, the fractional cirrus cloud amount is not interpreted literally. Instead, the LSM assumes 100% cirrus coverage and uses the fractional cirrus cloud amount to scale the cloud's optical depth. Thus all DWL "shots" would yield returns from cloud material and pass, attenuated, through to lower levels.

If the cloud is opaque and it is the first level that an opaque cloud is present, the LSM uses the cloud's fractional amount to randomly decide the DWL's opportunity of getting a cloud return or an aerosol/molecular return. For subsequent cloud levels, the opportunity is dependent upon whether the cloud is contiguous or not. If contiguous, then only the additional amount of cloud in the DWL's view is randomly considered. If the cloud is non-contiguous, then the potential of cloud amount that is in the DWL view is randomly distributed in order to compute the amount of additional cloud present at the level.

SWA studies are ongoing to test whether the overlap function algorithms are appropriate for the finer WRF resolutions.

2.2.3.4 CLOUD POROSITY MODEL

Based upon data returned from NASA's LITE mission (Winkler and Emmitt, 1998), the porosity of clouds appear to be greater than expected. Initial analysis suggest that, while nearly 80% of all DWL single "shots" are effected by water/ice clouds, 50% of those single "shots" are also able to provide a

PBL (or ground return). This characterization is sufficiently more optimistic than previous expectations to merit the inclusion of a "porosity" algorithm into the LSM.

Preliminary runs with extreme values for porosity (0-50%) illustrated the non-linear effects that this parameter has on the quality and quantity of wind data products. Since SWA is continuing to evaluate the cloud porosity model before any claims of realism can be defended, we have decided not to use this option at this time as default.

2.2.3.5 CLOUD OPTICAL PROPERTY MODEL

All opaque cloud backscatter values are preset in the LSM to be $1x10^{-06}$ m-1 sr-1 for 9 μm and $1.86x10^{-05}$ for 2 μm. We believe this value is properly conservative, since recent mid-layer cloud backscatter, measured with a lidar in the Antarctic, range from $1x10^{-06}$ to $1x10^{-04}$ m-1 sr-1 (Del Guasta et al., 1993).

OPAQUE CLOUD ATTENUATION COEFFICIENTS

Cloud Type	**Liquid Water Content**	**2 Micron (km^{-1})**	**9 Micron (km^{-1})**
Stratus I	0.22	2.33	13.16
Stratus II	0.05	0.43	2.52
Stratocumulus I	0.14	1.44	8.22
Stratocumulus II	0.47	4.70	24.96
Nimbostratus	0.50	4.88	26.34
Alto-stratus	0.28	3.01	16.94
Fair Weather Cumulus	1.0	9.26	46.45
Cumulonimbus	2.5	18.79	59.42

Opaque cloud absorption coefficients are based upon Stephens (1979) as a function of liquid water content and cloud type as shown below.

For cirrus cloud layers, cirrus backscatter is based on Northeastern University's cirrus model and is a function of cirrus cloud temperature as shown below.

CIRRUS CLOUD BACKSCATTER COEFFICIENTS

Temperature (deg C)	**9 Micron (m^{-1} sr^{-1})**	**2 Micron (m^{-1} sr^{-1})**
-60	$5.0x10^{-8}$	$1.5x10^{-6}$
-37	$9.0x10^{-7}$	$7.0x10^{-5}$
0	$9.0x10^{-7}$	$7.0x10^{-5}$

The cirrus cloud attenuation model is a modified version of an analytical AFGL cirrus algorithm found in the AFGL models (Kneizys et al., 1996 ; Gallery et al., 1983), where

$$\tau = e^{-0.14 \cdot L^2}$$

where

τ - the cirrus transmittance

L - the cirrus cloud thickness.

Since the LSM is restricted to the coarse vertical resolution of the Nature Run, the LSM uses the cirrus cloud percentage as a surrogate for cloud optical thickness.

The major assumption is that while the models derive a percent cirrus cloud coverage (i.e., 30%) from an average relative humidity within a grid volume, it is just as reasonable to interpret a thickness tendency from the same fields. Instead of using the percent coverage as literally meaning that 30% of the grid has cirrus cloud and 70% is totally cloud-free, the LSM assumes that the whole grid area is covered by a cirrus cloud that has an optical thickness that scales to the percent coverage. The cirrus cloud attenuations is defined as

$$\mathbf{ci_{\alpha} = 10^{\alpha} \cdot (CLD_{\%} \cdot 10)^2}$$

where

ci_{α} - the cirrus cloud attenuation

α - the AFGL cirrus attenuation coefficient for a 1 km thick layer

$CLD_{\%}$ - the cirrus cloud percentage cover.

Until new requests and funding is made, the DLSM version assigns the closest wavelength's cloud optical property value for wavelengths outside of the 2 to 9 μm range.

2.2.4 TURBULENCE MODELS

The DLSM has two options for estimating the wind variance on the sub-grid scale of the model. The first method computes the wind variance on the grid scale (9 x 9 x 9) and then scaling the variance to smaller scales by the Von Karman relationship. This “reasonable” approach has been used on Earth for many years but has not been fully verified by real data. The second method represents the uncertainties by scaling them to 20 % of the mean model wind speed. Comparisons of the uncertainties on Earth with the NMC rawinsonde profiles suggest that the simulated variances using the 20 % rule are not unreasonable. The user can also choose not to include turbulence.

2.2.4 TERRAIN

The T511 based GADS contain terrain information (based upon Geopotential height) at the 0.35 degree x 0.35 degree resolution.

2.3 DOPPLER WIND LIDAR MODEL

The LSM simulates the performance of coherent and direct detection Doppler wind lidars as space-based or airborne remote wind sensors with an emphasis upon realistic representations of the atmosphere along individual line of sights. The current optical property data bases support 2.0518 m coherent lidars and 0.355 μm, 0.532 μm and 1.06 μm direct detection lidars. Planned future upgrades to the optical property modules will support lidar wavelengths ranging from 0.3-1.6 μm range.

2.3.1 COHERENT SIGNAL PROCESSING MODELS

The LSM has the option to use a narrow band signal to noise model or a consensus curve algorithm for signal processing of the lidar signal.

2.3.1.1 COHERENT DWL SIGNAL PROCESSING MODEL: POLY-PULSE PAIR METHOD

There are several signal-to-noise (SNR) equations that have been suggested for use with Doppler lidar wind sounders. The narrow band SNR equation that the LSM uses is:

$$SNR_N = (c \cdot \pi \cdot \eta_1 \cdot \eta_2 \cdot \eta_3 \cdot \eta_4 \cdot J \cdot D^2 \cdot \tau \cdot \beta \cdot e^{-2 \int \alpha(r)dr}) \;/\; (8 \cdot h\nu \cdot (R^2 + (0.25 \cdot D^2/\lambda)^2))$$

where

- c - speed of light (m/s)
- η_1 - heterodyne quantum efficiency
- η_2 - optical efficiency
- η_3 - beam shape factor
- η_4 - truncation factor
- J - fundamental laser energy per pulse (Joules)
- D - mirror diameter (m)
- τ - pulse length (sec)
- β - backscatter (m^{-1} sr^{-1})
- $e^{-2 \int \alpha(r)dr}$ - 2 way attenuation
- $h\nu$ - photon energy (J)
- R - slant range (m)
- λ - laser wavelength (m)

As with the lidar SNR equation, there are several radial or LOS velocity error estimates, σ_{los}, that have been suggested for use with Doppler lidar wind sounders. While the Cramer-Rao Lower Bound may provide a limit to the extraction of a velocity estimate from a noisy signal, we have the option to chose the more conservative estimate based upon pulse pair autocorrelation processing of the Doppler signal. The following is derived from Eq. (6.22a) in Doviak and Zrnic (1984).

$$\sigma_{los} = (\lambda/4\pi \cdot f^{0.5}/2t) \times (2\pi^{1.5} \cdot W + 16 \cdot \pi^2 \cdot W^2/SNR_w + 1/SNR_w^{\,2})^{0.5}$$

where

- λ - wavelength (m)
- V_{max} - maximum velocity measured
- f - sampling frequency = $2 \cdot V_{max}/\lambda$
- t - pulse duration (sec)

W - normalized frequency spread of return signal (m/s) = $((V_{bw}^{2} + V_{atm}^{2})/(f\cdot \lambda))^{0.5}$

V_{bw} - uncertainty due to pulse bandwidth (m s^{-1})

V_{atm} - uncertainty due to turbulent eddies and wind shear within the pulse volume

$$SNR_w = \sqrt{2\pi} \cdot W \cdot SNR_N$$

2.3.1.1 COHERENT DWL SIGNAL PROCESSING MODEL: PHI-CAPON METHOD

A simplified version of the Effective Gaussian Signal Spectrum Model (Frehilch and Sharman, 2003; Frehilch, 1997; Frehilch, 1996) is used to estimate the performance of a coherent DWL for general conditions in the threshold regime of weak signals.

The wide band SNR equation used in the LSM is defined as

$$SNRW = (\pi \cdot \eta_1 \cdot \eta_2 \cdot \eta_3 \cdot \eta_4 \cdot \eta_5 \cdot J \cdot D^2 \cdot \lambda^2 \cdot \beta \cdot e^{-2\int \alpha(r)dr})/(8 \cdot h\nu \cdot 2 \cdot V_{max} \cdot R^2)$$

where

η_1 - heterodyne quantum efficiency

η_2 - transmit optical efficiency

η_3 - receive optical efficiency

η_4 - mixing efficiency

η_5 - coherent system margin

J - fundamental laser energy per pulse (Joules)

D - mirror diameter (m)

β - backscatter (m^{-1} sr^{-1})

$e^{-2\int \alpha(r)dr}$ - 2 way attenuation

$h\nu$ - photon energy (J)

R - slant range (m)

λ - laser wavelength (μm)

V_{max} - signal velocity bandwidth.

An effective wideband SNR (db) is computed by accumulating all the samples in an user's defined grid volume.

$$SNRW_{eff} = 10 \cdot \log10((\Sigma(SNRW_i)^2)^{0.5})$$

The number of data samples per LOS range gate is given as

$$m = (2.0 \cdot d \cdot 2.0 \cdot V_{max}) / (c \cdot \lambda \cdot 1E\text{-}6)$$

where

- λ - wavelength (m)
- V_{max} - maximum velocity measured
- c - speed of light (m/s)
- d - range gate (m).

Thus the effective photons per LOS range gate is

$$\phi = m \cdot SNRW_{eff}.$$

The percentage of bad estimates described by the following fraction of random outliers is

$$B = \exp(-(0.1 \cdot \phi / B_0)^{\alpha})$$

where

- B_0 - constant
- α - constant

The percentage of bad estimates is used to decided whether the DWL performance produces a failed attempt, false alarm or a good wind measurement. If B is greater than the user's entry of the gross error probability threshold, then it is considered a failed attempt. If the performance is considered to be a "good" performance, then the estimates have a random chance of producing a false alarm in which ϕ is set to 0.1. The line of sight uncertainty spread for the "good" estimates is defined as

$$\sigma_{los} = C \cdot (1.0 + (\phi \cdot 0.1 / G_0)^{\varepsilon})^{(-\delta)} + \mu$$

where

- σ_{los} - the line-of-sight uncertainty (m/s)
- X - constant
- G_0 - constant
- ε - constant
- δ - constant
- μ - constant.

2.3.2 DWL SIGNAL PROCESSING MODEL: DIRECT DETECTION DOUBLE EDGE

A simplified version of the double edge technique model (Flesia and Korb, 1999; Korb et al., 1992) is used to estimate the performance of a direct detection DWL. The direct detection number of source photons reaching the beam splitter is defined as

$$N_{photons} = (\pi \cdot \eta_1 \cdot \eta_2 \cdot \eta_3 \cdot \eta_4 \cdot \eta_5 \cdot \eta_6 \cdot J \cdot C_\lambda \cdot D^2 \cdot \lambda \cdot \beta \cdot e^{-2 \int \alpha(r)dr}) / (4 \cdot Pk \cdot c \cdot R^2)$$

where

- η_1 - detector quantum efficiency
- η_2 - transmit optical efficiency
- η_3 - receive optical efficiency up to detector subsystem edge filters
- η_4 - fraction of signal sent to each of the edge filters (beam split fraction)
- η_5 - engineering adjustment factor
- η_6 - edge filter throughput for source (aerosol or molecular) signal
- **J** - fundamental laser energy per pulse (Joules)
- C_λ - wavelength conversion factor
- **D** - mirror diameter (m)
- β - backscatter (m^{-1} sr^{-1})
- $e^{-2 \int \alpha(r)dr}$ - 2 way attenuation
- **Pk** - plank constant
- **c** - speed of light (m/s)
- **R** - slant range (m)
- λ - laser wavelength (μm)

The DLSM accumulates the photons and dark noise photon counts for the user's grid volume as follows

$$\psi = \Sigma((\zeta \cdot 100.0) \cdot d / c)$$

$$\gamma = \Sigma\, N_{photons} \cdot d$$

where

- ψ - noise photocounts from the dark current in the detector
- ζ - dark current photocounts/s
- **c** - speed of light (m/s)
- **d** - range gate (m)
- $N_{photons}$ - number of source photons reaching the beam splitter
- γ - accumulated source photons reaching the beam splitter

Assuming that aerosol/molecular ratio is very small and both edges have the same throughput, the effective SNR and LOS uncertainty along the edge are described as

$$SNR_e = \gamma/(1.0 + (\psi/\gamma))\sigma_{los} = (2/SNR_e)^{0.5} / \varepsilon_s$$

where

SNR_e - effective SNR along the edge

ε_S - edge sensitivity

σ_{los} - LOS uncertainty along the edge

The DLSM has an photon count module that counts photons for aerosols (and clouds) and molecules at the primary mirror's focus post atmospheric effects as follows

$$\xi_1 = \Sigma(\pi \cdot \eta_2 \cdot J \cdot C_\lambda \cdot D^2 \cdot \lambda \cdot \beta_a \cdot e^{-2\int \alpha(r)dr})/(4 \cdot Pk \cdot c \cdot R^2) \cdot d$$

$$\xi_2 = \Sigma(\pi \cdot \eta_2 \cdot J \cdot C_\lambda \cdot D^2 \cdot \lambda \cdot \beta_m \cdot e^{-2\int \alpha(r)dr})/(4 \cdot Pk \cdot c \cdot R^2) \cdot d$$

where

β_a - aerosol backscatter ($m^{-1}sr^{-1}$)

β_m - molecule backscatter ($m^{-1}sr^{-1}$)

ξ_1 - accumulated aerosol photons at the primary mirror's focus post atm. effects

ξ_2 - accumulated molecule photons at the primary mirror's focus post atm. effects

2.3.3 FRINGE IMAGER

A simplified version of the Fringe Imager model (Skinner and Hays, 1994) is used to estimate the performance of a direct detection DWL.

(The Fringe Imager model algorithm is currently not integrated into the DLSM version 4.4)

2.3.4 OPTICAL AUTOCOVARIANCE WIND LIDAR (OAWL)

In 2013, SWA constructed a conceptual model for a space-based OPTICAL AUTOCOVARIANCE WIND LIDAR (OAWL) with Ball Aerospace & Technologies Corp. Ball and SWA worked to complete an OAWL performance model that was integrated into the DLSM. The DLSM addressed key questions and concepts for OAWL and produced simulated products for OSSEs conducted at NCEP and AOML. This model is currently proprietary to Ball Aerospace & Technologies Corp.

2.4 LINE-OF-SIGHT WIND PRODUCTS

For each DWL line of sight perspective, a profile of forward model winds at each range gate is computed using the input horizontal wind components from the "Nature Run" (converted to along track and cross track perspectives), platform geometry and the sampling scale uncertainties.

$$V_{for} = ((U_{ct}+\sigma_u \cdot GN) \cdot \cos(\theta)+(V_{at}+\sigma_v \cdot GN)\sin(\theta))\cos(\phi)+W_{vv}+(\sigma_w \cdot GN)\sin(\phi)$$

where

V_{for} - the forward model line-of-sight wind velocity (m/s)

U_{ct} - the cross track wind velocity at the shot location (m/s)

σ_u - the sampling scale uncertainty in the cross track wind (m/s)

GN - gaussian distributed random number

θ - heading angle (rad)

V_{at} - the along track wind velocity at the shot location (m/s)

σ_v - the sampling scale uncertainty in the along track wind (m/s)

ϕ - the elevation angle (rad)

W_{vv} - the vertical velocity at the shot location (m/s)

σ_w - the sampling scale uncertainty in the vertical velocity (m/s)

The simulated DWL line-of-sight wind velocity is calculated by adding the line-of-sight uncertainty derived from the DWL's signal-to-noise model to the forward model wind as follows:

$$V_{los} = V_{for} + \sigma_{los}$$

where

V_{los} - the line-of-sight wind velocity (m/s)

σ_{los} - the line-of-sight uncertainty (m/s).

2.5 DWL SHOT ACCUMULATION (GRID VOLUME AVERAGING)

The Lidar Simulation Model estimates the performances of a pulsed DWL for a user-defined grid volume in order to define a lidar measurement of the line of sight wind. The LSM supports two methods; single measurement LOS accumulation and multiple measurement volume accumulation.

Single shot mode: Along each DWL line of sight, each pulse within the user's defined vertical thickness resolution (with respect to the ABL) is accumulated to contribute to the DWL LOS wind estimate as depicted in the following figure:

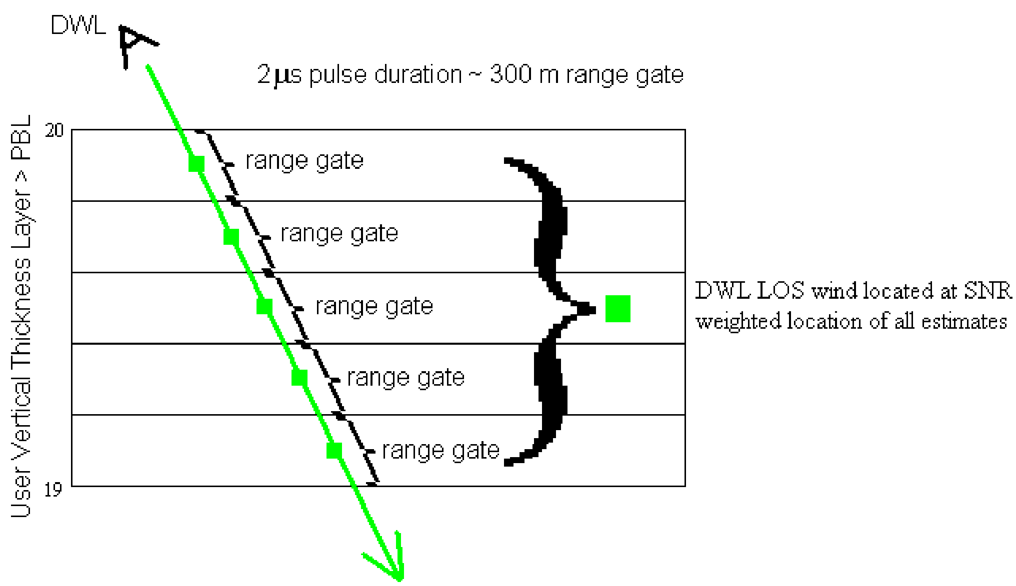

Accumulation Mode: The method the DLSM accumulates each pulse over an user-defined grid volume depends upon the user's scan mode: either conical or step/stare.

For a conically scanned DWL, the grid volume is defined horizontally by the user's angle bin and number of scans for shot accumulation (shown in figure below) and the previously discussed vertical accumulation. Since this configuration is not likely and is only included in the DLSM for statistical purposes, the user is strongly cautioned when using this option.

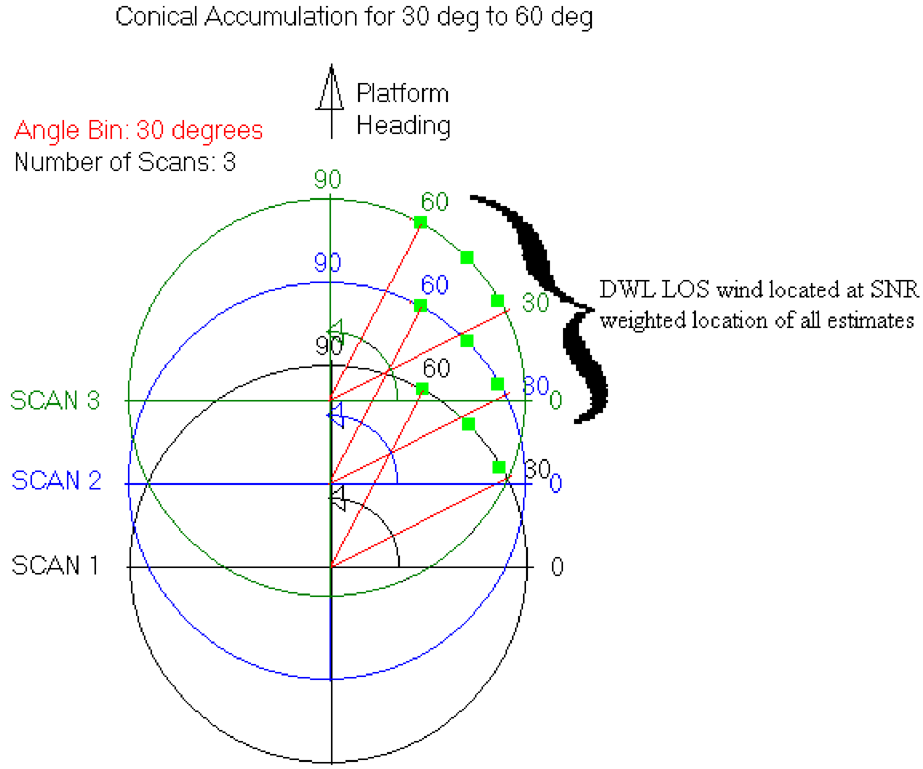

For step/stare DWL, the grid volume is defined horizontally by each dwell time of the stare and the previously discussed vertical accumulation. The percentage of shots to accumulate in a stare is preset to 100% in the DLSM Version 4.4

2.5.1 A VERTICAL EXAMPLE

Consider the following as an simple example of the disposition of 20 shots as they pass through the lowest 20 km of the earth's atmosphere. Assume 10 DWL 'shots' per azimuth perspective (forward and aft) in two stares. The LSM computes the single shot DWL LOS winds from backscattering sources such as aerosols, molecules and clouds. Each backscattering source and perspective is considered to provide a unique measurement in each grid volume. A single representation of the wind in each grid volume for each source and perspective is computed by accumulating the single shot DWL LOS estimates. The LSM also computes the standard deviation of the accumulated single shot LOS winds. This standard deviation reflects not only system accuracy, but also representativeness as long as the single shots are distributed throughout the grid volume. The target data product is a single LOS for each of the two perspectives within a volume defined by the dwell time of the stare and a vertical thickness above the PBL of 1 km. In this example the global atmospheric model (eg ECMWF) calls for 25% cloud coverage at 8 km, 50% coverage at 4 km and 40% coverage at 2 km.

At 8 km the clouds are taken to be cirrus, but the 25% coverage is not interpreted literally. Instead, we assume 100% cirrus coverage and use the value of 25% to scale the optical depth between 0 and 1.4 km. Thus all 20 shots would yield returns, 10 "forward" and 10 "aft", from cloud material at 8 km and pass, attenuated, through to lower levels. The two sets of 10 shots would be processed to produce one LOS wind speed for each perspective. The DWL LOS height assignments are SNR weighted and are usually near the top of the cirrus layer.

For the non-cirrus clouds at 4 km, the 50% coverage is taken literally. Hence, 5 forward/5 aft shots are intercepted by cloud and 5 forward/5 aft shots provide aerosol returns. In this case, the two LOS wind speeds (forward and aft) computed for the 1 km thickness layer are dominated by the cloud's presence. The DWL LOS height assignments are SNR weighted and are usually near the top of the cloud layer. Only the shots that missed the clouds continue on to lower levels.

At 2 km, the opaque cloud is non-contiguous with respect to the 4 km cloud layer. The DLSM uses the satellite view cloud overlap function to determine how much of the cloud is viewable. In this case consider fifty percent of the 40% impacts the DWL "shots". 1/1 shots are processed to provide two DWL LOS winds from a cloud dominate volume and as before the DWL LOS height assignments are SNR weighted and are usually near the top of the cloud layer. 4/4 shots continue on to yield aerosol and surface returns.

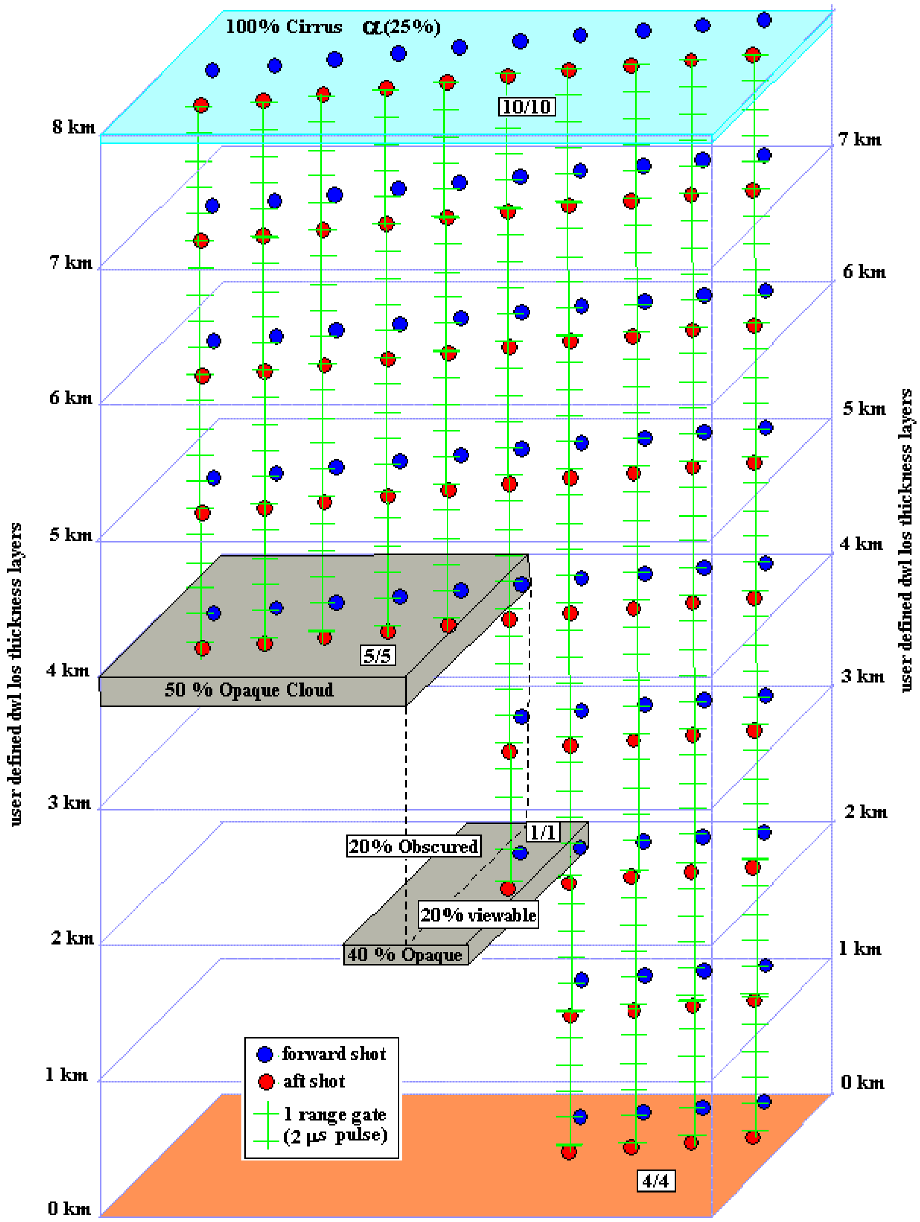

2.5.2 ADDITIONAL DOPPLER SHIFT EFFECTS

Additional Doppler shift effects that are computed for direct detection lidars by the DLSM 4.4 are the molecular Gaussian broadening, the Lorentzian aerosol broadening, the Doppler shift due to Earth's motion and the Doppler shift due to Satellite's motion. The LOS wind models assume that the Earth and the satellite motion effects have been corrected for and therefore are not included in the wind calculations.

The DLSM 4.4 outputs the grid volume average of atmospheric temperature, the molecular Gaussian broadening function and the Lorentzian aerosol broadening function (Skinner and Hays, 1994) to the DLSM's PHT output file. The Lorentzian aerosol broadening functions are provided for very small, small , and large size aerosol sizes including Doppler shift information from the LOS wind, LOS wind and Earth motion and LOS wind plus Earth motion plus satellite motion.

2.5.2.1 MOLECULAR GAUSSIAN BROADENING FUNCTION

The Molecules have a Gaussian broadening function is defined as

$$\Delta\nu_G = 4.3X10^{-7}\cdot\nu\cdot(T/M)^{1/2}$$ eq.8 of Skinner and Hayes

where

$\Delta\nu_G$ - Rayleigh broadening

ν - wavenumber (cm^{-1})

T - average temperature (K)

M - mean molecular weight (28.964)

For example, a typical Rayleigh width at a temperature, 250 K, and a wavelength, 0.355 μm is $3.56X10^{-2}$ cm^{-1}.

2.5.2.2 LORENTZIAN AEROSOL BROADENING FUNCTION

The aerosol broadening function is a Lorentzian form defined as

$$L_a(\Delta\nu,\alpha_a) = 1/\pi\cdot\alpha_a / (\alpha_a^2 + \Delta\nu^2)$$ eq.9 of Skinner and Hayes

$$\alpha_a = (2\pi\cdot\nu^2\cdot D) / (c\cdot mcm)$$ eq.10 of Skinner and Hayes

$$\Delta\nu = \nu\cdot(2\cdot U\cdot\sin(\phi)/c)$$ eq.4 of Skinner and Hayes

where

$L_a(\Delta\nu,\alpha_a)$ - aerosol broadening function

α_a - half width

ν - wavenumber (cm^{-1})

D - diffusion coefficient (cm^2/s)

c - speed of light (m/s)

mcm - meters to centimeters conversion factor

$\Delta\nu$ - Doppler shift due to mean wind motions (cm^{-1})

U - the horizontal wind speed in the direction of the viewing (m/s)

ϕ - angle from nadir the beam makes as it passes through the atmospheric layer (rad)

The DLSM 4.4 outputs to the PHT file the Lorentzian aerosol broadening for the following three aerosol radius sizes and diffusion coefficients.

Particle Radius (μm)	Diffusion Coefficient (cm^2/s)
10^{-2}	$1.3x10^{-4}$
10^{-1}	$2.2x10^{-6}$
10^{0}	$1.3x10^{-7}$

2.5.2.3 DOPPLER SHIFT DUE TO EARTH MOTION AND THE SATELLITE MOTION

In addition, the DLSM 4.4 outputs to the PHT file the Lorentzian broadening for Doppler shift due to earth's motion and the Lorentzian broadening for Doppler shift due to earth's motion plus Doppler shift due to satellite motion .

The Doppler shift due to Earth's motion is defined as

$$V_e = (UX \cdot \cos(\beta) + VX \cdot \sin(\beta))\cos(\phi)$$

where

- V_e - Doppler Shift Due to Earth's Motion (m/s)
- **UX** - cross track component of the Earth's rotation speed (m/s)
- **VX** - along track component of the Earth's rotation speed (m/s)
- β - DWL azimuth scan angle (rad)
- ϕ - DWL nadir scan angle (rad)

The Doppler shift due to Satellite's motion is defined as

$$V_s = \sin(\beta) \cdot \sin(\phi) \cdot V_{sat}$$

where

- V_s - Doppler Shift Due to Satellite's Motion (m/s)
- V_{sat} - Satellite velocity (m/s)
- β - DWL azimuth scan angle (rad)
- ϕ - DWL nadir scan angle (rad)

2.6 SIMULATED LOS PRODUCTS

2.6.1 LOS WIND OUTPUT RECORDS

Model Line of Sight (LOS) outputs consist of averages and standard deviations of variables related to the DWL measurements accumulated in the user defined grid volume. For comparison purposes, the LSM's LOS file provides simulated LOS wind products for grid cells with and without cloud effects. The DLSM LOS output files are in ASCII format.

average of the along track input wind components (m/s)
standard deviation of the along track input wind components (m/s)
average of the cross track input wind components (m/s)
standard deviation of the cross track input wind components (m/s)

average of the velocity input wind components (m/s)
standard deviation of the velocity input wind components (m/s)
average of the sub-grid scale uncertainty for the cross track component (m/s)
standard deviation of the sub-grid scale uncertainty for the cross track component (m/s)
average of the sub-grid scale uncertainty for the along track component (m/s)
standard deviation of the sub-grid scale uncertainty for the along track component (m/s)
average of the sub-grid scale uncertainty for the vertical velocity component (m/s)
standard deviation of the sub-grid scale uncertainty for the vertical velocity component (m/s)
average of the forward model LOS wind (m/s)
standard deviation of the forward model LOS wind (m/s)
signal weighted average of the platform latitude (deg) - cloud effects included
signal weighted standard deviation of the platform latitude (deg) - cloud effects included
signal weighted average of the platform longitude (deg) - cloud effects included
signal weighted standard deviation of the platform longitude (deg) - cloud effects included
signal weighted average of the platform heading (deg) - cloud effects included
signal weighted standard deviation of the platform heading (deg) - cloud effects included
signal weighted average of the platform altitude (km) - cloud effects included
signal weighted standard deviation of the platform altitude (km) - cloud effects included
signal weighted average of the sequential time (s) - cloud effects included
signal weighted standard deviation of the sequential time (s) - cloud effects included
signal weighted average of the azimuth scan angle (deg) - cloud effects included
signal weighted standard deviation of the azimuth scan angle (deg) - cloud effects included
signal weighted average of the nadir scan angle (deg) - cloud effects included
signal weighted standard deviation of the nadir scan angle (deg) - cloud effects included
signal weighted average of the elevation angle (deg) - cloud effects included
signal weighted standard deviation of the elevation angle (deg) - cloud effects included
signal weighted average of the latitude (deg) - cloud effects included
signal weighted standard deviation of the latitude (deg) - cloud effects included
signal weighted average of the longitude (deg) - cloud effects included
signal weighted standard deviation of longitude (deg) - cloud effects included
signal weighted average of the height assignment (km) - cloud effects included
signal weighted standard deviation of the height assignment (km) - cloud effects included
signal weighted average of the Range (km) - cloud effects included
signal weighted standard deviation of the Range (km) - cloud effects included
number of estimates in grid volume - cloud effects included
number of estimates above user set thresh hold in grid volume - cloud effects included
average of the backscatter (m-1 sr-1) - cloud effects included
standard deviation of the backscatter (m-1 sr-1) - cloud effects included
average of the attenuation (km-1) - cloud effects included

standard deviation of the attenuation (km-1) - cloud effects included
average of the transmission - cloud effects included
standard deviation of the transmission - cloud effects included
average of the SNRw or sum of the dark noise - cloud effects included
standard deviation of the SNRw - cloud effects included
average of the effective SNRw or sum of the photons - cloud effects included
source medium indicator - cloud effects included
shot passed indicator (0-no 1-yes) - cloud effects included
shot failed indicator (0-no 1-yes)- cloud effects included
shot false alarm indicator (0-no 1-yes) - cloud effects included
consensus LOS uncertainty (m/s) - cloud effects included
along the LOS uncertainty (m/s) - cloud effects included
target volume error (instant LOS uncertainty) (m/s) - cloud effects included
DWL LOS wind velocity (m/s) - cloud effects included
forward LOS wind minus the DWL LOS wind (m/s) - cloud effects included
signal weighted average of the platform latitude (deg) - cloud effects not included
signal weighted standard deviation of the platform latitude (deg) - cloud effects not included
signal weighted average of the platform longitude (deg) - cloud effects not included
signal weighted standard deviation of the platform longitude (deg) - cloud effects not included
signal weighted average of the platform heading (deg) - cloud effects not included
signal weighted standard deviation of the platform heading (deg) - cloud effects not included
signal weighted average of the platform altitude (km) - cloud effects not included
signal weighted standard deviation of the platform altitude (km) - cloud effects not included
signal weighted average of the sequential time (s) - cloud effects not included
signal weighted standard deviation of the sequential time (s) - cloud effects not included
signal weighted average of the azimuth scan angle (deg) - cloud effects not included
signal wted. standard deviation of the azimuth scan angle (deg) - cloud effects not included
signal weighted average of the nadir scan angle (deg) - cloud effects not included
signal weighted standard deviation of the nadir scan angle (deg) - cloud effects not included
signal weighted average of the elevation angle (deg) - cloud effects not included
signal weighted standard deviation of the elevation angle (deg) - cloud effects not included
signal weighted average of the latitude (deg) - cloud effects not included
signal weighted standard deviation of the latitude (deg) - cloud effects not included
signal weighted average of the longitude (deg) - cloud effects not included
signal weighted standard deviation of longitude (deg) - cloud effects not included
signal weighted average of the height assignment (km) - cloud effects not included
signal weighted standard deviation of the height assignment (km) - cloud effects not included
signal weighted average of the Range (km) - cloud effects not included
signal weighted standard deviation of the Range (km) - cloud effects not included

number of estimates in grid volume - cloud effects not included
number of estimates above user set thresh hold in grid volume - cloud effects not included
average of the backscatter (m-1 sr-1) - cloud effects not included
standard deviation of the backscatter (m-1 sr-1) - cloud effects not included
average of the attenuation (km-1) - cloud effects not included
standard deviation of the attenuation (km-1) - cloud effects not included
average of the transmission - cloud effects not included
standard deviation of the transmission - cloud effects not included
average of the SNRw or sum of the dark noise - cloud effects not included
standard deviation of the SNRw - cloud effects not included
average of the effective SNRw or sum of the photons - cloud effects not included
source medium indicator - cloud effects not included
shot passed indicator (0-no 1-yes) - cloud effects not included
shot failed indicator (0-no 1-yes) - cloud effects not included
shot false alarm indicator (0-no 1-yes) - cloud effects not included
consensus LOS uncertainty (m/s) - cloud effects not included
along the LOS uncertainty (m/s) - cloud effects not included
target volume error (instant LOS uncertainty) (m/s) - cloud effects not included
DWL LOS wind velocity (m/s) - cloud effects not included
forward LOS wind minus the DWL LOS wind (m/s) - cloud effects not included
average of the PBL height (km)

2.6.1 MODEL LINE OF SIGHT PHOTON COUNTS

Model Line of Sight photon count file (PHT) consist of average direct detection pre-detector variables related to the DWL measurements accumulated in the user defined grid volume. The DLSM PHT output files are in ASCII format.

Grid volume weighted average of the platform latitude (deg)
Grid volume weighted average of the platform longitude (deg)
Grid volume weighted average of the platform heading (referenced from 0 east Mathematic (deg))
Grid volume weighted average of the platform altitude (km)
Geometric thickness of the atmospheric layer of the grid volume (m)
Grid volume weighted average of the sequential time (s)
Grid volume weighted average of the azimuth scan angle (deg)
Grid volume weighted average of the nadir scan angle (deg)
Grid volume weighted average of the elevation angle (deg)
Grid volume weighted average of the DWL LOS wind latitude (deg)
Grid volume weighted average of the DWL LOS longitude (deg)
Grid volume weighted average of the DWL LOS height assignment (km)

Grid volume weighted average of the range from satellite to DWL LOS wind (km)
Grid volume number of DWL estimates in grid volume
source medium (1- aerosol/molecules, 2- opaque cloud, 3 – cirrus cloud)
Grid volume average source backscatter coefficient (log (x) (m-1 sr-1))
Grid volume average non-source backscatter coefficient (log (x) (m-1 sr-1)) (aerosols for molecules DWL, molecules for aerosol DWL)
Grid volume average source attenuation coefficient (km-1)
Grid volume average transmission (-)
Grid volume dark noise count
Grid volume photon count at primary mirror for source
Grid volume photon count at primary mirror for non-source (aerosols for molecules DWL, molecules for aerosol DWL)
Grid volume average temperature (K)
Grid volume Doppler shift due to satellite motion
Grid volume Doppler shift due to earth motion
Grid volume rayleigh broadening
Grid volume aerosol broadening for .01 µm aerosol radii (based upon LOS Doppler motion)
Grid volume aerosol broadening for 0.1 µm aerosol radii (based upon LOS Doppler motion)
Grid volume aerosol broadening for 1 µm aerosol radii (based upon LOS Doppler motion)
Grid volume aerosol broadening for .01 µm aerosol radii (based upon LOS Doppler motion plus Doppler shift due to earth motion)
Grid volume aerosol broadening for 0.1 µm aerosol radii (based upon LOS Doppler motion plus Doppler shift due to earth motion)
Grid volume aerosol broadening for 1 µm aerosol radii (based upon LOS Doppler motion plus Doppler shift due to earth motion)
Grid volume aerosol broadening for 0.01 µm aerosol radii (based upon LOS Doppler motion plus Doppler shift due to earth and sat. motion)
Grid volume aerosol broadening for 0.1 µm aerosol radii (based upon LOS Doppler motion plus Doppler shift due to earth and sat. motion)
Grid volume aerosol broadening for 1 µm aerosol radii (based upon LOS Doppler motion plus Doppler shift due to earth and sat. motion)

2.6.2 SIMULATED HORIZONTAL WIND PRODUCTS

The LSM uses either the Multi-Paired Algorithm (MPA) or a Least Squares technique (Press et al., 1986) to compute the U and V horizontal wind components from the DWL line-of-sight velocities. The horizontal wind products are computed with one of three different models: High Resolution model, Grid Area Model using the MPA and Grid Area Model using the Least Squares model. Sampling and measurement errors are computed in each horizontal wind model.

The MPA matches forward and aft lidar line-of-sight wind velocities to compute weighted horizontal wind components. The MPA weights the winds by angular separation from orthogonality and by the distance between the lidar shots (Emmitt and Wood, 1988) as shown below.

$$\alpha_{wt} = 1.0 - ((\pi/2 - (\beta_\alpha - \beta_\phi))\cdot(2/\pi))^4$$

$$D_{wt} = 1-(((\phi_a\cdot\Theta_c\cdot\cos(\Theta_a) - \phi_f\cdot\Theta_c\cdot\cos(\Theta_f))^2 + ((\Theta_a + 90)\cdot\Theta_c - (\Theta_f + 90)\cdot\Theta_c)^2)^{½})/D$$

where

- α_{wt} - angle shot pair weight
- D_{wt} - distance shot pair weight
- Θ_c - degrees to kilometers conversion factor at equator (111.11) (km/deg)
- D - diagonal distance across the grid area (km)
- ϕ_a - longitude of the aft shot (deg)
- ϕ_f - longitude of the forward shot (deg)
- Θ_a - latitude of the aft shot (deg)
- Θ_f - latitude of the forward shot (deg)

The U and V horizontal wind components are computed, respectively, as follows:

$$U = ((VLOS_a / (\cos(\Theta)\cdot\cos(\beta_\alpha)) - (VLOS_f\cdot\tan(\beta_\alpha))) /$$

$$(\cos(\Theta)\cdot\sin(\beta_\phi))/(1.0 - \tan(\beta_\alpha)/\tan(\beta_\phi))$$

$$V = (VLOS_a - U\cdot\cos(Q)\cdot\cos(\beta_a))/(\cos(\Theta)\cdot\sin(\beta_a))$$

where

- U - U horizontal wind component (m/s)
- V - V horizontal wind component (m/s)
- $VLOS_a$ - line-of-sight lidar wind for aft shot (m/s)
- $VLOS_f$ - line-of-sight lidar wind for forward shot (m/s)
- Θ - elevation angle (deg)
- β_a - scanner angle for aft shot (deg)
- β_f - scanner angle for forward shot (deg).

An analytical expression for the MPA errors dependent upon shot separation was derived. The line-of-sight (LOS) velocities for two shots from different perspectives can be expressed as follows:

$$VLOS_1 = (U_1\cdot\cos\Phi_1 + V_1\cdot\sin\Phi_1)\cdot\sin\Theta + W_1\cdot\cos\Theta + N_1$$

$$VLOS_2 = (U_2 \cdot \cos\Phi_2 + V_2 \cdot \sin\Theta_2) \cdot \sin\Theta + W_2 \cdot \cos\Theta + N_2$$

where

- $VLOS_i$ - line-of-sight velocity for shot (m/s)
- U_i - u component of the wind at location (m/s)
- V_i - v component of the wind at location (m/s)
- W_i - w component of the wind at location (m/s)
- N_i - random noise
- Φ_i - azimuth for shot i from mathematic +x (deg)
- Θ - elevation angle from the nadir (deg)

Given the scarcity of shots, the following assumptions are made to solve for the horizontal wind components

$$u_1 = u_2 ; v_1 = v_2 ; w_1 = w_2 = 0.0 ; \Phi_2 = -\Phi_1 ; N_1 = N_2 = 0$$

Thus:

$$VLOS_1 = (U \cdot \cos\Phi_1 + V \cdot \sin\Phi_2) \cdot \sin\Theta$$

$$VLOS_2 = (U \cdot \cos\Phi_2 + V \cdot \sin\Phi_2) \cdot \sin\Theta$$

To get two equations in two unknowns (**u,v**) we substitute Q_1 for Q_2:

$$VLOS_1 = (u \cdot \cos\Phi_1 + v \cdot \sin\Phi_1) \cdot \sin\Theta$$

$$VLOS_2 = (u \cdot \cos\Phi_1 - v \cdot \sin\Phi_1) \cdot \sin\Theta$$

Solving for **u**:

$$VLOS_1 + VLOS_2 = 2 \cdot u \cdot \cos\Phi_1 \cdot \sin\Theta$$

$$u = (VLOS_1 + VLOS)/(2 \cdot \cos\Phi_1 \cdot \sin\Theta)$$

Solving for **v**:

$$VLOS_1 - VLOS_2 = 2 \cdot v \cdot \sin\Phi_1 \cdot \sin\Theta$$

$$v = (VLOS_1 - VLOS_2)/(2 \sin\Phi_1 \cdot \sin\Theta)$$

However, if U_2,U_1 and V_2, V_1 then we make the following substitution:

$$U_2 = U_1 + u$$

$$V_2 = V_1 + v$$

$$VLOS_2 = (u \cdot \cos\Phi_2 + v \cdot \Phi_2) \cdot \sin\Theta + (u \cdot \cos\Theta_2 + v \cdot \sin\Phi_2) \cdot \sin\Theta$$

$$= (u \cdot \cos\Phi - v \sin\Phi) \cdot \sin\Theta + (u \cdot \cos\Phi - v \cdot \sin\Phi) \cdot \sin\Theta$$

Solving for **u** and **v**:

$$u = (VLOS_1 + VLOS_2)/(2 \cdot \cos\Phi \cdot \sin\Theta) + (\delta u/2 - (\delta v \cdot \tan\Phi)/2$$

$$v = (VLOS_1 - VLOS_2)/(2 \cdot \sin\Phi \cdot \sin\Theta) - (\delta u)/(2\tan\Phi) + (\delta u)/2$$

The correct **u** and **v** values would be **u + ½ u** and **v + ½ v**. Therefore, the errors due to having different horizontal velocities at shot locations 1 and 2 are:

$$U_{error} = - \delta v \cdot \tan\Phi/2$$

$$V_{error} = - \delta u/2 \cdot \tan\Phi$$

If **u** and **v** are statistically non-zero (i.e., related to some coherent structure) then there will be a residual error regardless of the number of shots used in the velocity estimates. We can compute the average u and v errors for a given shot pair spacing.

2.6.2.1 HIGH RESOLUTION METHOD

The high resolution method uses the MPA to match the closest aft line-of-sight shot with the closest forward line-of-sight shot to produce a simulated horizontal U, V wind product. Each shot pair is weighted by angular separation, distance between shots and SNR.

2.6.2.2 MPA GRID-BASED METHOD

The MPA Grid-Based Method uses the MPA to match all aft line-of-sight shots with all forward line-of-sight shots in the user defined grid area cell size to produce a simulated horizontal U, V wind product. Each shot pair is weighted by angular separation, distance between shots and SNR.

2.6.2.3 LEAST-SQUARES GRID-BASED METHOD

The least squares model performs a least squares fit to the lidar shots within the user's defined grid area to produce SNR weighted U and V horizontal wind components (Press et al., 1986).

2.6.2.4 DLSM HORIZONTAL WIND OUTPUT PRODUCTS

DLSM Horizontal Wind Output Products
Number of shot pairs (or samples) used to make wind estimates
User defined altitude (km)
Laser wind altitude (km)
Weighted laser wind latitude (deg)

Weighted laser wind longitude (deg)
Weighted time of the laser wind (sec)
Weighted U horizontal wind component (m/s)
Weighted V horizontal wind component (m/s)
Average total weight (0-1)
Average SNR weight (0-1)
Average angle weight (0-1)
Average distance weight (0-1)
Average real U wind component at weighted wind location (m/s)
Average real V wind component at weighted wind location (m/s)
Average LOS uncertainty at weighted wind location (m/s)

3.0 REFERENCES

Atlas, R and G. D. Emmitt. Simulation studies of the impact of space-based wind profiles on global climate studies. Proc. AMS Sixth Symp. on Global Change Studies, Dallas , TX , January, 1995.

Baker, W.E., G.D. Emmitt, F. Robertson, R.M. Atlas, J.E. Molinari, D.A. Bowdle, J. Paegle, R.M. Hardesty, R.T. Menzies, T.N. Krishnamurti, R.A. Brown, M.J. Post, J.R. Anderson, A.C. Lorenc and J. McElroy. Lidar-measured winds from space: A key component for weather and climate prediction. Bull. Amer. Meteor. Soc., 76, 869-888, 1995.

Betts, A.K. A new convective adjustment scheme, Part I: Observational and theoretical basis. Quart. J. Roy. Meteor. Soc., 112, 1306-1335, 1986.

Black, T.L. The new NMC Mesoscale ETA model: Description and forecast examples. Wea. and Forec., 9, 265-278, 1994.

Del Guasta, M., M. Morandi and L. Stifanutti. One year of cloud lidar data from Dumont d'Urville (Antarctica), 1. General overview of geometrical and optical properties. J. Geophys. Res., 98, 18575-18587, 1993.

Doviak, R.J. and D.S. Zrnic. Doppler Radar and Weather Observations, Academic Press, New York, 458 pp., 1984.

Emmitt, G.D. and S.A. Wood, 2001: Simulating space-based lidar performance using global and regional scale atmospheric numerical models. Optical Remote Sensing Topical Mtg., Coeur d' Alene , ID , February.

Emmitt, G.D. and S.A. Wood. Lidar Mapping of Cloud Tops and Cloud Top Winds, 1996. PL-TR-96-2129, F19628-93-C-0196, 1996

Emmitt, G.D. and S.A. Wood. Simulating clouds within a space-based Doppler lidar wind sounder simulation model. Paper presented at the Cloud Impacts on DOD Operations and Systems 1995 Conference, Hanscom AFB/Phillips Laboratory, October, 1995.

Emmitt, G.D., S.A. Wood and M. Morris. Space-based Doppler lidar sampling strategies -- algorithm development and simulated observation experiments. Report under NASA Contract NAS8-37779, Marshall Space Flight Center, 1990.

Emmitt, G. D. and S. A. Wood. Influence of Coherent Mesoscale Structures on Satellite-Based Doppler Lidar Wind Measurements II. NASA Contract # NAS8-36902, Final Report, 1988.

Emmitt, G. D. Doppler Lidar Sampling Strategies and Accuracies-- Regional Scale. Presented at the Symposium and Workshop on Global Wind Measurements, Aspen, CO, 1987.

Flesia, C. and C. Korb. Theory of the double-edge molecular technique for Doppler lidar wind measurement. Appl. Opt., 38, 432-440, 1999.

Frehilch, R. and B. Sharman, Predicting Effects of Wind Variability on Doppler Lidar Performance. Presented at the Lidar Working Group Meeting, Oxnard, Ca, 2003.

Frehilch, R., Effects of Wind Turbulence on Coherent Doppler Lidar Performance. J. Atmos. Oceanic. Technol., 14, p54-74., 1997

Frehlich, Rod "Coherent Doppler Lidar Measurements of Winds," in "Trends in Optics: Research, Developments and Applications," Anna Consortini, editor, Academic Press, 1996

Gallery, W.O., F.X. Kneizys and S.A. Clough. Air mass computer program for atmospheric transmittance/radiance calculation: FSCATM. AFGL-TR-83-0065, 1983, ADA132108.

Greco, S., S. Wood, G. Emmitt, M. Nicholls and R. Pielke, Sr., 2000: Lidar simulations over hurricane Bonnie using CAMEX-3 data, a lidar simulation model and numerical model analyses. AMS 24th Conf. Hurr. Trop. Meteor., Ft. Lauderdale , FL , May.

Hanel, G. Computation of the extinction of visible radiation by atmospheric aerosol particles as a function of the relative humidity based upon measured properties. Aerosol Sci., 3, 377-386, 1972.

Hess, S. L. Introduction to Theoretical Meteorology, Holt, Rinehart and Winston, New York, pp. 201-205, 1979.

Houston, S. H. and G.D. Emmitt. Impact to a Space-based Doppler Lidar Wind Profiler on our Knowledge of Hurricanes and Tropical Meteorology. Presented at the AMS 17th Conference on Hurricanes and Tropical Meteorology, Miami, FL, 1986.

Kells, L.M., W.F. Kern and J.R. Bland. Plane and Spherical Trigonometry, McGraw-Hill Book Company, New York, 2nd ed., pp. 309-321, 1940.

Kneizys, F. X., L. W. Abreu, G. P. Anderson, J. H. Chetwynd, E. P. Shettle, D. C. Robertson, P. Acharya, L.S. Rothman, J. E. A. Selby, W. O. Gallery, and S. A. Clough. The MODTRAN 2/3 Report and LOWTRAN 7 Model, Phillips Laboratory, Geophysics Directorate, Hanscom AFB, Ma, F19628-91-C-0132, 1996.

Korb C., B. Gentry, and C. Y. Weng, The Edge Technique - Theory and application to the Lidar Measurement of Atmospheric Winds. Applied Optics, 31, pp 4202-4212, 1992.

Lord, S. L., M. Masutani, J. C. Woollen, J. C. Derber, G. D. Emmitt, S. A. Wood, S.Greco, J. Terry, R. Atlas, and T. J. Kleespies. Impact Assessment of a Doppler Wind Lidar for NPOESS/OSSE. Presented at the AMS Sixth Symposium on Integrated Observing Systems.13-17 January 2002, Orlando Florida.

Mellor, G.L. and T. Yamada. Development of a turbulence closure model for geophysical fluid problems. Rev. Geophys. Space Phys., 20, 851-875, 1982.

Menzel, W.P., D.P. Wylie and K.L. Strabala. Seasonal and diurnal changes in cirrus cloud as seen in four years of observations with the VAS. J. Appl. Meteor., 31, 370-385, 1992.

Masutani, M, J. S. Woollen,S.J. Lord, T. J. Kleespies, G. D. Emmitt, H. Sun, S. A. Wood, S. Greco, J. Terry, R. Treadon, K. A. Campana, 2006 :
Observing System Simulation Experiments at NCEP. NCEP Office note No.451. August 2006

Pratte, J. F. and R. W. Lee. A short method of Generating Meteorological Fields for Simulation Studies. J. Appl. Meteor., 18, 1670-1674.

Press, W. H., B. P. Flannery, S. A. Teukolsky, W. T. Vetterling. Modeling of Data, In Numerical Recipes: The Art of Scientific Computing, Chap. 14, Cambridge Press, New York, pp. 498-546, 1986

Rhyne, R. H., H. Murrow, and K. Sidwell. Atmospheric Turbulence Power Spectral Measurements to Long Wavelengths for Several Meteorological Conditions, Presented at NASA Conference, Hampton, VA, pp. 271-286, 1976.

Riishojgaard, L. P., Z. Ma, M. Masutani, J. S. Woollen, G. D. Emmitt, S. A. Wood, and S. Greco, 2012: Observation System Simulation Experiments for a Global Wind Observing Sounder, Geophys. Res. Lett., 39, L17805, doi: 10.1029/2012GL051814.

Skinner W. R. and P.B. Hays. A Comparative Study of Coherent & Incoherent Doppler Lidar Techniques. Contract NAS 8-38775, U. of Michigan for NASA Marshall Space Flight Center (MSFC), 3 June 1994.

Slingo, J.M. The development and verification of a cloud prediction scheme for the ECMWF model. Quart. J. Roy. Meteor. Soc., 113, 899-927, 1987.

Srivastava, V. , J. Rothermel, A. D. Clarke, J. D. Spinhirne, R.T. Menzies, D.R. Cutten, M.A. Jarzembski, D.A. Bowdle, and E.W. McCaul, 2001: Wavelength dependence of backscatter by use of aerosol microphysics and lidar data sets: application to 2.1um wavelength for space-based and airborne lidars. Applied Optics, V40, 4759-4769.

Stephens, G.L. Optical properties of eight water cloud types. CSIRO Aust. Div. Atmos. Phys. Tech. Pap. No. 36, 1-35, 1979.

Stowe, L.L., H.Y.M. Yeh, T.F. Eck, C.G. Wellenmeyer, H.L. Kyle and the Nimbus-7 Cloud Data Processing Team. Nimbus-7 global cloud climatology, Part III. First year results. J. Clim., 2, 671-709, 1989.

Winkler, D. and G. D. Emmitt. 1998: Cloud statistics from LITE and relevance to wind lidar performance. Presented at the NOAA Working Group on Space-Based Lidar Winds, Boulder, CO, July 13-16., 1998.

Wood, S.A., G.D. Emmitt and S. Greco, 2014: Simulation testbeds for the assessment of space-based wind measuring systems. SPIE Remote Sensing at Amsterdam, NL. Conference 9241: Sensors, Systems, and Next-Generation Satellites [9241-64], Sep 22-15.

Wood, S., G.D. Emmitt, and S. Greco, 2001: The challenges of accessing the future impact of space-based Doppler wind lidars while using today's global and regional atmospheric models. AMS 5th Symp. Integrated Observing Systems, Albuquerque , NM , January.

Wood, S., G. Emmitt and S. Greco, 2000: DLSM: A coherent and direct detection lidar simulation model for simulating space-based and aircraft-based lidar winds. Proceedings SPIE's 14th Annual Internat. Symp. Aerospace Defense Sensing, Simulation and Controls, Orlando , FL , April.

Wood, S. A., G. D. Emmitt. and S. Greco. Optical Remote Sensors as Components of an Airborne Hurricane Observing System. Presented at the American Meteorological Society Conference, Long Beach, Ca, 1997.

Wood, S.A., G.D. Emmitt, D. Bai, L.S. Wood and S. Greco. A coherent lidar simulation model for simulating space-based and aircraft-based lidar winds. Paper presented at the Optical Society of America's Coherent Laser Radar Topical Meeting, Keystone, CO, July, 1995.

Wood, S.A., G.D. Emmitt, M. Morris, L. Wood and D. Bai. Space-based Doppler lidar sampling strategies -- algorithm development and simulated observation experiments. Final Rept. NASA Contract NAS8-38559, Marshall Space Flight Center, 266 pp., 1993.

Wood, S. A. and G. D. Emmitt. A Reference Atmosphere for LAWS Trade Studies: An Update. Presented at the American Meteorological Society Conference, New Orleans, LA, 1991.

Wood, S. A. and G. D. Emmitt. A Reference Atmosphere for LAWS Trade Studies. Presented at The Optical Remote Sensing of the Atmosphere Topical Meeting, Lake Tahoe, NV, 1990.

Woodbury, G.E. and M.P. McCormick. Zonal and geographical distributions of cirrus clouds determined from SAGE data. J. Geophys. Res., 91, 2775-2785, 1986.

Zhao, Q., F.H. Carr and G.B. Lesins. Improvement of precipitation forecasts by including cloud water in NMC's Eta model. Preprints Amer. Meteor. Soc. Ninth Conf. Num. Wea. Pred., Denver, CO, pp. 50-53, 1991.